

Plant/Control Optimization of a PEM Hybrid Fuel Cell Vehicle to Grid (V2G) System

Final Report
April 19th, 2007

Dongsuk Kum
Scott Moura

ME 555 – Winter 2007
Professor Panos Y. Papalambros

Abstract

Combined plant/control optimization is applied to a PEM hybrid fuel cell vehicle (HFCV) for vehicle to grid (V2G) applications. The HFCV model is developed from past control-oriented models. For the purposes of design optimization, three components (fuel cell stack, compressor, and battery) are made scalable. To construct a control scheme suitable for combined plant/control design optimization, a rule-based method is selected and framed in a manner such that several key parameters are formulated as design variables. Simulation based computations of the objective function are characterized by noise, and therefore inappropriate for gradient-based optimization algorithms. A surrogate modeling method is suggested using neural networks to approximate the physical model. Using the surrogate model, the combined design and controller HFCV model is optimized for maximum fuel economy for a given stationary power demand cycle. The solution is analyzed with respect to various optimality properties, such as constraint activity, Lagrange multipliers, interior & bounded solutions, and varying starting points. The trade-offs between optimal design solutions and constraints is observed and analyzed to analyze optimal design solutions for a PEM HFCV operating as an energy source to the power grid. Multi-objective optimization problems are formulated through parametric studies to elucidate trade offs between different design objectives. A resultant set of “design rules” are formulated to provide a physical engineering interpretation of the conclusions found.

Table of Contents

1. Introduction.....	3
1.1 V2G Background	3
1.2 Problem Statement	3
2. Nomenclature.....	4
2.1 Symbols.....	4
2.2 Common Subscripts	4
3. PEM Hybrid Fuel Cell System Model	5
3.1 Fuel Cell System	5
3.1.1 Fuel Cell Stack.....	6
3.1.2 Compressor	7
3.1.3 Auxiliary Components	8
3.2 Battery.....	8
3.3 Rule-Based Control Algorithm	10
3.4 System Level Block Diagram	12
3.5 Grid Power Demand Cycle	12
4. Optimization Problem Formulation	14
4.1 Objective Function.....	14
4.2 Design Variables.....	14
4.3 Constraints	15
4.4 Model Parameters	20
4.5 Optimization Problem Summary	20
5. Model Analysis	21
5.1 Dynamic Simulation	22
5.2 Design of Experiments Study	23
5.3 Monotonicity Analysis.....	26
5.4 Surrogate Modeling through Neural Networks.....	28
6. Optimization Study	30
6.1 Optimization Results.....	30
6.2 Constraint Activity.....	31
6.3 Lagrange Multipliers.....	33
6.4 Interior vs. Boundary Solutions	35
6.5 Variation of Starting Points	37
6.6 Surrogate Model Feasibility.....	39
7. Parametric Study.....	41
7.1 Minimum SOC.....	41
7.2 Maximum Battery Weight	42
7.3 Maximum Fuel Cell Stack Length.....	43
8. Discussion of Results	44
8.1 Design Rules	44
8.2 Model Limitations.....	45
8.3 Future Work	45
9. Acknowledgements.....	46
10. References.....	47

1. Introduction

1.1 V2G Background

The fuel cell vehicle fleet and electric power grid are remarkably complementary as systems for managing energy. Proton exchange membrane (PEM) fuel cells produce energy with nearly twice the efficiency of internal combustion engines [1]. Fuel cells also hold the potential to generate power locally and from a wide variety of energy sources. This presents an opportunity to leverage the power generating and absorbing capacity of a hybrid fuel cell vehicle (HFCV) to help load balance localized grid segments while simultaneously increasing grid stability and reliability. This concept is widely known as Vehicle to Grid (V2G). The objective of this project is to study the combined plant and controller design for a PEM hybrid fuel cell vehicle operating as an energy source for stationary power. The subsequent analysis will provide insight to the inherent trade-offs between applying a mobile power plant design as an energy source for the power grid.

1.2 Problem Statement

Engineering literature is rich with topics on combined design and control optimization of fuel cell systems for either mobile [2-4] or stationary use. However V2G has motivated the investigation of a PEM hybrid fuel cell system intended for *both* applications. Moreover, HFCV optimization is characterized by a combined plant/control design problem. Past researchers have developed first-order necessary conditions for optimality by combining the Karush-Kuhn-Tucker conditions from optimization theory and Bellman-Pontryagin conditions from control theory [5]. However, such derivations are beyond the scope of this project. We investigate past work [2-4] and extend the study of combined optimization to a HFCV operating as a power source for the grid. Although hybrid fuel cell systems have been optimized for stationary or mobile purposes separately, trade-offs arise in the design of a system intended for vehicle to grid application. These trade-offs include component sizing and operating efficiency, among others. Stationary fuel cell power systems have no constraints on size or weight, whereas these parameters are critical for on-board vehicular applications. In addition, the power demand for driving cycles is typically twice the amount required for a single household. Therefore one might expect a HFCV designed for driving cycles would likely function outside of its optimal operating region when

plugged into the grid. As a result, the optimal design requires a delicate balance between satisfying requirements for grid power, yet maintaining a design feasible for on-board vehicle applications. Although it would be very interesting to optimize for both applications and analyze the design trade-off between stationary and mobile applications, this report focuses solely on the stationary optimization problem.

2. Nomenclature

2.1 Symbols

A	Area	f	Objective function
E	Voltage	g	Inequality constraint
K_{ch}	Battery charge control gain	h	Equality constraint
L	Length	k	Discrete time-step
M	Weight	m	Mass
P	Power	n	Number of components
Q	Heat transfer	n_{FC}	Number of fuel cells in stack
SOC	Battery state of charge	p	Pressure
T	Temperature	t	Thickness
V	Volume	x	Design variables
W	Mass flow rate		
α	Rule-based controller gain		
Δ	Displacement		
η	Efficiency		
κ	Motor parameter or orifice constant		
λ, μ	Lagrange multiplier		
λ	Ratio		

2.2 Common Subscripts

AN	Anode	H_2	Hydrogen
atm	Atmospheric	in	Inlet
$batt$	Battery	max	Maximum
dem	Demand	min	Minimum
des	Desired	out	Outlet
FC	Fuel cell	pa	Power assist mode
CA	Cathode	SM	Supply manifold
CP	Compressor	req	Requested
CM	Compressor motor	RM	Return manifold

3. PEM Hybrid Fuel Cell System Model

In order to formulate a suitable optimization problem, an analysis model is required to feed responses back to the optimization algorithm, given a set of design variables. The performance of the given set of design variables is evaluated by the optimization algorithm, which then feeds a new set of design variable back to the optimization algorithm. This iterative process continues until the optimization algorithm is able to converge to an optimal solution. This section discusses the separate subsystems that comprise the overall PEM hybrid fuel cell system model used for analysis. The optimization problem formulation is discussed in the following section.

3.1 Fuel Cell System

Accurately modeling a fuel cell system is a non-trivial process, involving considerations for the electrochemistry, hydrogen and air manifolds, membrane water content, flow control/supercharging devices, vehicle inertia dynamics, and cell/stack temperatures [6]. Clearly, preparing a mathematical systems-level model based on first principles can be a formidable task, reflected by the relative lack of publications in this area. The most widely used and studied model existing in the literature was developed in a control oriented fashion by Pukrushpan *et al.* [7]. Since the model was developed specifically for vehicle control studies, certain dynamic effects were included and others neglected, based upon the relative time constant of each phenomenon. This model has both advantages and limitations with respect to simulation accuracy and complexity. A first principles approach to system dynamics guarantees a level of validity at the cost of computational efficiency. Moreover, the model is limited in its applicability as the parameter values are based on an antiquated Ford P2000 fuel cell. Nevertheless, this model is popular among the controls community and has been shown to deliver reasonably accurate results. A summary of the principles used in the development of individual components, including the fuel cell stack, compressor, and other auxiliary components provides a general background for the system under study. Some equations are shown for simple illustration and others omitted for simplicity. The reader can refer to [7] for detailed derivations and explanations of all components and sub-models.

3.1.1 Fuel Cell Stack

The fuel cell stack model contains four interacting sub-models, including the stack voltage, anode flow, cathode flow, and membrane hydration model. The stack voltage model is comprised of an open circuit voltage and three types of losses. The open circuit voltage is computed from the energy balance between chemical energy in the reactants and electrical energy formed. The chemical reaction which takes place in the cell is given by



The energy produced can be computed by the Gibbs free energy and Nernst voltage equation. However, this only represents the so-called open circuit voltage and in reality losses occur. These losses are represented by an activation loss, ohmic loss, and concentration loss. In total, the sum of the voltage created and lost forms the cell terminal voltage, given by Equation (2). The fuel cell polarization curve shown in Figure 1 provides a visual representation of the cell voltage created with respect to current density.

$$E_{oc} - E_{act} - E_{ohm} - E_{conc} \quad (2)$$

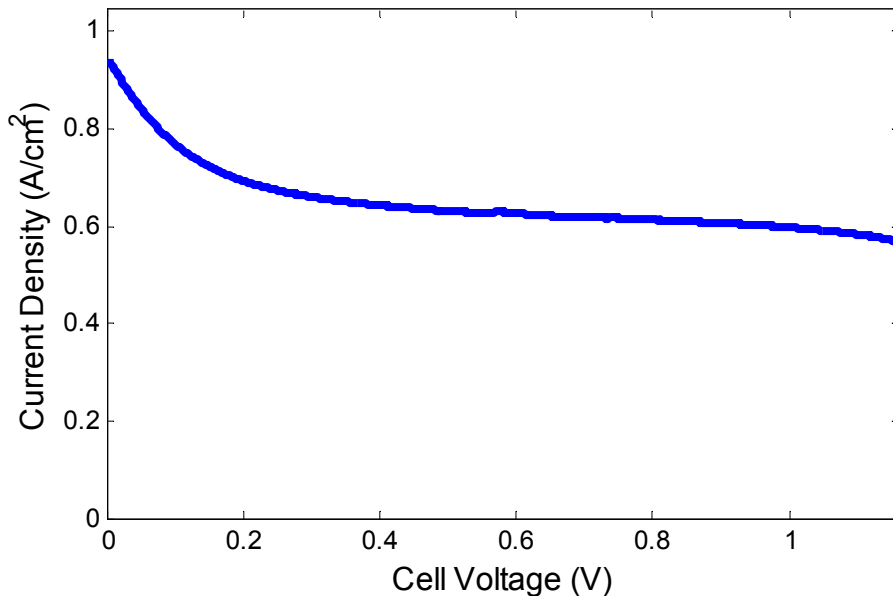


Figure 1: Fuel cell polarization curve generated from model developed in [6]

The cathode mass flow models capture the dynamic effects of air flow behavior as it enters the stack. The equations used in the development of this model use the principles of mass

conservation, thermodynamics, and psychometric properties of air. The three dynamic states within this sub-model include the masses of oxygen, nitrogen, and water vapor.

Similar to the cathode sub-model, the anode mass flow model uses the principles of mass continuity, thermodynamics, and psychometric properties. However, the anode mass flow contains hydrogen as opposed to air. The dynamics states in the anode are the masses of hydrogen and water.

A membrane hydration model serves the purpose of predicting the water content within the membrane and mass flow rate of water across the membrane. Some very significant assumptions are made, including that the mass flow is assumed to be uniform across the overall surface area of the membrane.

3.1.2 Compressor

The compressor model is separated into two components: compressor & compressor motor inertia dynamics and an efficiency map. The dynamics are modeled by a lumped rotational inertia model representing the compressor and motor masses. Applying Euler-Newton equations results in a single state given by the rotational speed of the compressor. Mass flow rate characteristics are modeled using the Jensen & Kristensen method [8]. Compressor efficiency is derived using curve fitting methods for data obtained from an Allied Signal compressor. The efficiency map takes the pressure ratio across the compressor and mass flow rate as inputs.

$$\eta_{CP} = f\left(\frac{P_{SM}}{P_{atm}}, W_{CP}\right) \quad (3)$$

Although the data for this particular map is derived from a single compressor's performance, Han suggests that similarity rules can easily be applied to adjust the efficiency map when scaling compressor size [2]. The inputs to the efficiency map scale with compressor size according to

$$W_{scaled} = \lambda_{CP}^2 \cdot W \quad (4)$$

where λ_{CP} is a geometric scale factor defining the ratio of the scaled compressor size to the original. In a similar fashion, the power required by the compressor scales according to

$$P_{scaled,CP} = \lambda_{CP}^2 \cdot P_{CP} \quad (5)$$

This result is extremely useful with respect to selecting compressor scale as a design variable. This choice is discussed in further detail in subsequent sections.

3.1.3 Auxiliary Components

The remaining auxiliary components within the model include supply manifold, return manifold, cooler, and humidifier. Both manifolds are modeled as lumped volumes associated with the pipes and connections between each device. Since the pressure difference between the supply manifold and cathode is relatively small, a linear nozzle equation approximates the mass flow rate

$$W_{SM,out} = \kappa_{SM,out} (P_{SM} - P_{CA}) \quad (6)$$

Conversely, the return manifold experiences a relatively large pressure drop between the anode and atmosphere, therefore requiring a nonlinear nozzle equation. For simplicity, the equation is omitted here, since the goal is to highlight general modeling concepts and not exact equation derivations.

Air leaving the compressor is typically very hot and may damage the MEA. Hence, a cooler is utilized to reduce incoming air temperature to fuel cell stack operating temperature, $T_{st} = 80^{\circ}C$. Air flow is also humidified before entering the stack in order to ensure proper hydration of the MEA. This is performed by injecting water into the air mass flow. Simple psychometric properties and relations are leveraged to model this effect.

3.2 Battery

Another important component of the hybrid fuel cell system is the battery. The role of battery is to add the capability of storing excess energy and using it when needed, which allows great flexibility for energy management. The battery model is adapted from the ADVISOR energy storage system model. The system comprises of a single input and two outputs. The input signal is the amount of power charged or discharged from the battery. The model outputs include SOC and charge/discharge power limits. Numerically, positive power on the input port represents battery discharge, and conversely negative power represents battery charge. The ADVISOR battery model uses the resistive equivalent circuit model developed by the National Renewable Energy Laboratory (NREL), shown in Figure 2. This modeling framework provides sufficient

fidelity of the salient battery characteristics while enabling the use of mathematical equations to model system-level performance and efficiency. Two lumped parameters, R and V_{oc} are necessary to fully describe the characteristics of the battery. These two parameters are functions of SOC level and temperature. We, however, assume isothermal operations in this study for simplicity.

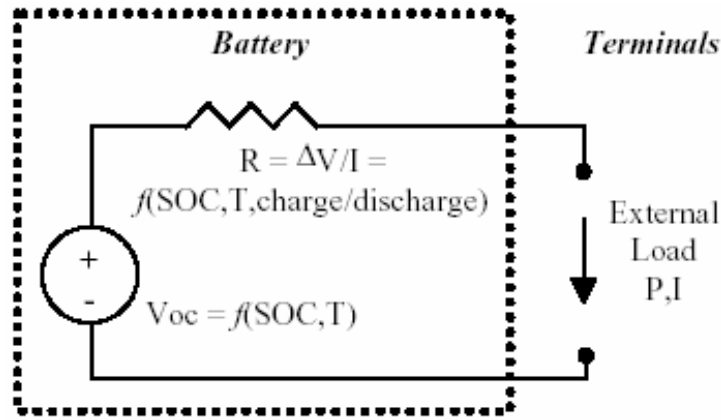


Figure 2: Resistive equivalent circuit model

The resistive equivalent circuit model leads to a set of algebraic equations, defining open circuit voltage and current through the resistor. To output SOC, current is integrated with respect to time, thus forming a first order dynamic system, as described in Equation (10). Following are the most significant equations needed for the model shown in Figure 2.

$$V_{oc} = f(SOC, T) \quad , \quad R_{int} = f(SOC, T) \quad (7)$$

$$P_{batt_lim} = f(P_{batt_req}, V_{oc}, R_{int}) \quad (8)$$

$$I_{batt} = -\frac{V_{oc} - \sqrt{V_{oc}^2 - 4P_{batt_lim}R_{int}}}{2R_{int}} \quad (9)$$

$$\dot{SOC} = -\frac{I_{batt}}{Q_{max}} \Rightarrow SOC = \frac{Q_{max} - \int I_{batt} dt}{Q_{max}} \quad (10)$$

Note that V and R are nonlinear functions of both SOC and temperature, forming a nonlinear map that defines the characteristics of the battery.

3.3 Rule-Based Control Algorithm

The rule-based control algorithm is employed to appropriately manage power flow between the fuel cell, battery, and grid. The main idea of the rule-based control is to operate the fuel cell within a desired operating region that achieves high efficiency as shown in Figure 3. In order for the fuel cell to operate in the desired region, the rule-based supervisory controller divides the hybrid fuel cell (FC) operation into three modes: battery only, power assist, and fuel cell only mode. In battery mode, the fuel cell is turned off and all power demand is supplied by the battery. This requires SOC to exist at a sufficient level and the power demand to be less than the battery power limit in order to provide necessary power. When there exists excessive power demand, fuel cell efficiency decreases if the fuel cell were to provide the necessary power alone. To alleviate this issue, the controller changes to power assist mode. In power assist mode, both the fuel cell and battery provide power. The fuel cell provides baseload power, defined by the power assist threshold, while the battery provides ancillaries, thus regulating operation to the high efficiency region. When power demand is moderate, the control scheme selects fuel cell only mode. In this mode, the fuel cell provides all power demand plus power to recharge the battery to its desired SOC level. As a consequence, the control scheme leverages the hybrid architecture to regulate fuel cell operation within a region of high efficiency by using the battery as a load leveling device.

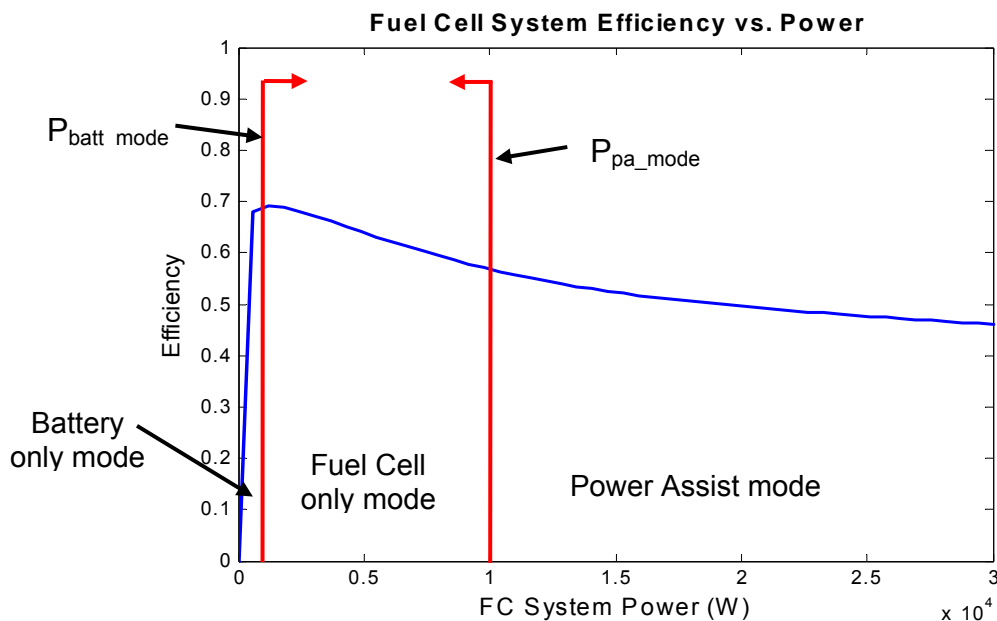


Figure 3: Fuel Cell operating regions determined by the rule-based controller

Following are the rules which govern the supervisory controller and compute necessary power request from each power source.

1. If $P_{dem} < P_{bat_mode}$ and $SOC > SOC_{lower_lim}$, then it is *battery only mode* and $P_{fc} = 0$,
 $P_{batt} = P_{dem}$
2. If $SOC > SOC_{lower_lim}$ and $P_{dem} > P_{fc_max}$, then it is *power assist mode* and $P_{fc} = P_{fc_max}$,
 $P_{batt} = P_{dem} - P_{fc}$
3. Otherwise, it is in *fuel cell only mode* and $P_{fc} = P_{dem} + P_{charge}$, $P_{batt} = -P_{charge}$, where
 $P_{charge} = \min(P_{bat_lim}, K_{chg} \cdot (SOC - SOC_{des}))$

Figure 4 visualizes rule-based algorithm described above using flow chart.

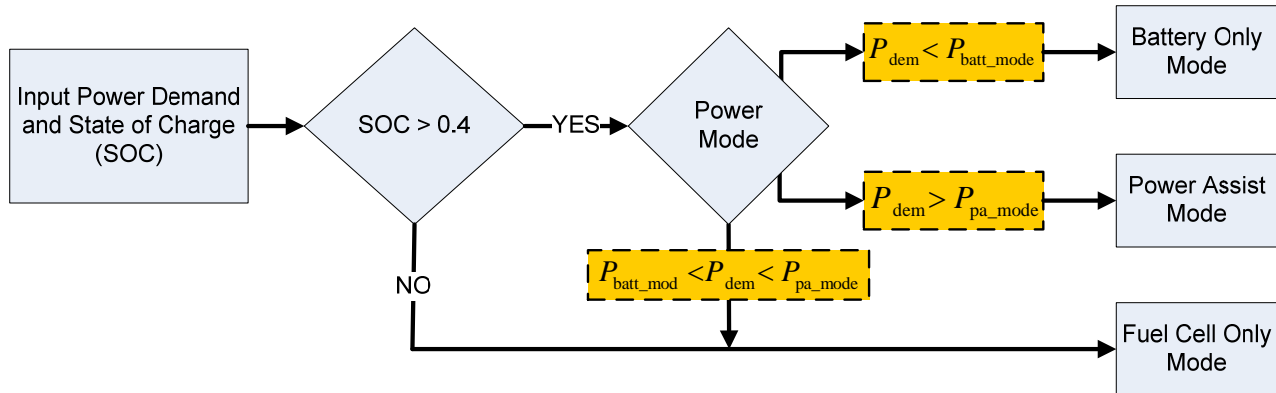


Figure 4: Rule-based supervisory controller algorithm flow chart

In block diagram representation, Figure 5 below shows the main inputs and outputs of the supervisory controller. The supervisory controller computes the necessary power request to both the fuel cell and battery using power demand and battery SOC as inputs.

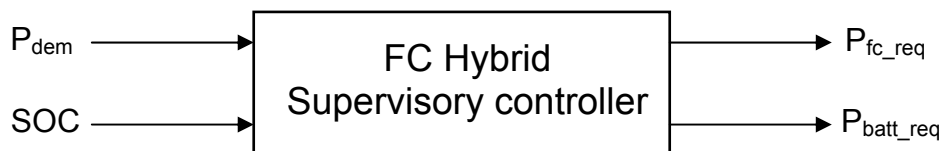


Figure 5: Input/Output of the FC hybrid supervisory controller

3.4 System Level Block Diagram

Figure 6 shows an overview of the complete system, including the supervisory controller. Wide arrows indicate the energy flow between components of the system, whereas the narrow arrows designate the direction of the input/output signal for the supervisory controller.

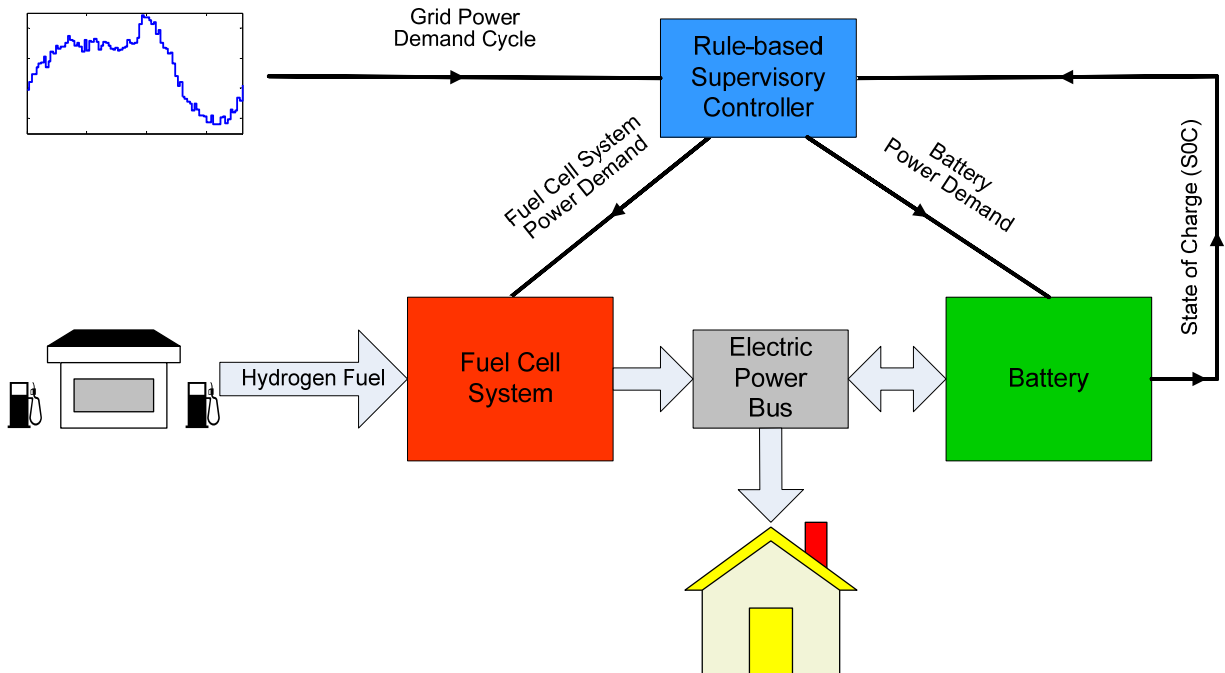


Figure 6: System level block diagram for energy flow and control signal

3.5 Grid Power Demand Cycle

In order to simulate a hybrid fuel cell system providing stationary power, a representative grid power demand cycle must be applied in similar fashion to using a drive cycle for mobile applications. This is accomplished by using the forecasted power demand on a typical weekday (Tuesday March 6, 2007) for the California power grid, as provided by the California Independent System Operator (CAISO). This data is easily obtained by logging onto the CAISO website at www.caiso.com [9]. A representative figure of the data provided by CAISO is provided in Figure 7.

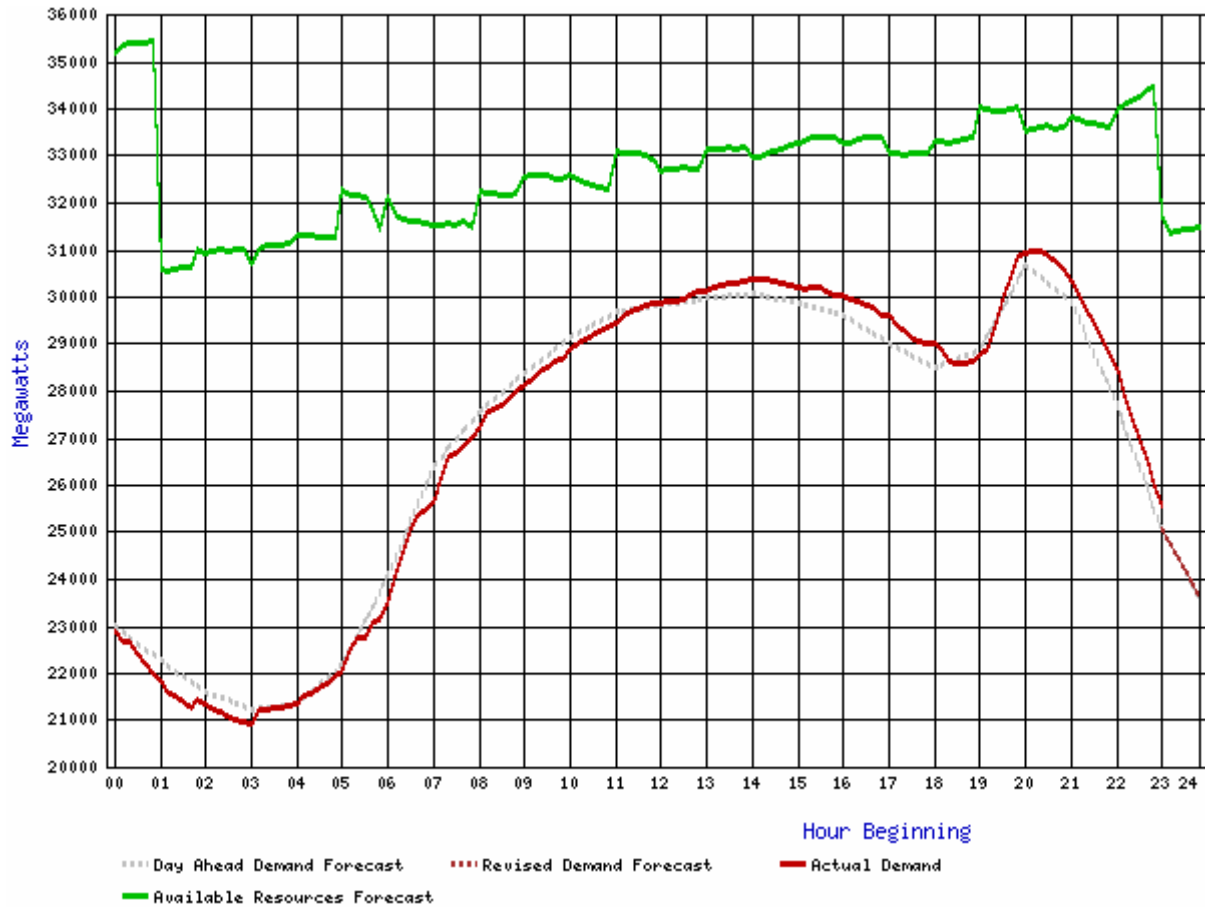


Figure 7: A single day power outlook for the California ISO control area. The forecasted power from Tuesday March 6, 2007 is utilized for development of the grid power demand cycle [9].

This data is modified in three stages to create a suitable power demand cycle. First, a continuous and smooth cycle is formed using a cubic spline on the data points. These values are then scaled down to power demand values that are on the order of magnitude for a typical office building or apartment complex. Second, a white Gaussian noise frequency distribution is superimposed on the cycle to model fast power demand changes, such as turning lights on and off, using a toaster oven, heated central air system, etc. In the third stage, the time scale is compressed from 24 hours to 720 seconds in order to create a feasible simulation time which contains the overall characteristics of a full day cycle. The resulting representative grid power demand cycle is shown in Figure 8 for a full day, from 6am to 6am.

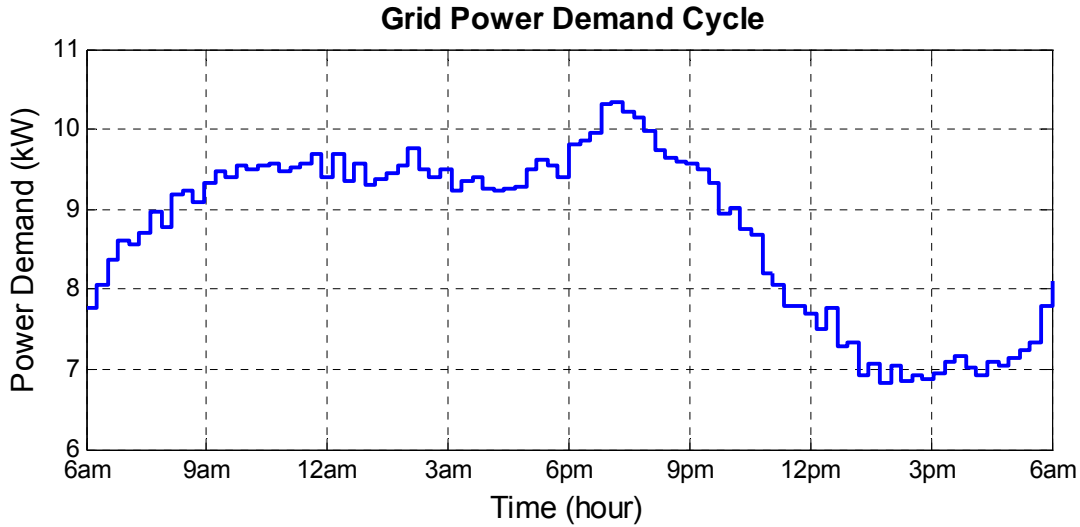


Figure 8: Scaled, splined grid power demand cycle with white Gaussian noise over 24 hour period. This cycle is compressed to 720 sec for simulation. [Source: Cal ISO Power Demand Forecast - Tuesday March 6, 2007]

4. Optimization Problem Formulation

4.1 Objective Function

The goal of the design optimization problem is to minimize the amount of hydrogen consumed while supplying power to the grid over a prescribed power demand profile. The objective function is minimized with respect to a set of component sizes and control variables,

$$\mathbf{x} = [\lambda_{CP} \quad n_{FC} \quad n_{BATT} \quad P_{pa} \quad P_{batt} \quad K_{ch}]^T.$$

$$\text{minimize } f(\mathbf{x}) = (\text{fuel_consumption}) = m_{H_2}(\lambda_{CP}, n_{FC}, n_{BATT}, P_{pa}, P_{batt}, K_{ch}) \quad (11)$$

The amount of hydrogen consumed is calculated from the system model, where m_{H_2} represents the total mass of hydrogen consumed by the system. The fuel cell model originally developed in [6] predicts transient behaviors such as compressor inertia dynamics, mass flows, partial pressures, and humidity. In total, this model includes nine states, which we assume accurately models the phenomena of interest.

4.2 Design Variables

The design variables, represented by vector \mathbf{x} , include compressor scale, λ_{CP} , number of fuel cells, n_{FC} , and number of battery modules, n_{BATT} , threshold power value for power assist mode, P_{pa} , threshold power value for battery only mode, P_{batt} , and battery charge control gain, K_{ch} .

Compressor size directly impacts the performance of the fuel cell. A larger compressor may increase air mass flow rate and power production. On the other hand, a larger compressor increases the rotational inertia of the blades and causes greater power drain due to auxiliary loads. Therefore, the exact value for compressor size must be chosen to carefully balance power vs. efficiency. The number of fuel cells within the stack, n_{FC} , clearly influences power production, efficiency, and total stack size. Selecting this value requires balancing each of these factors to adequately meet engineering goals. The number of battery modules, n_{BATT} , determines the battery’s level of participation for providing power. Like the number of fuel cells, this variable must balance power efficiency and weight. If the power demand exceeds P_{pa} , the rule-based supervisory control algorithm requests power from *both* the fuel cell and battery. This mode of operation is commonly referred to as “power assist.” If the power demand is less than P_{batt} , power is supplied by the battery alone. These two threshold values bound a region of high operating efficiency for the fuel cell. The final design variable K_{ch} acts as a control gain. It determines how fast to charge the battery, which will affect the *SOC* convergence rate of approaching SOC_{des} . These design variables form a six-dimensional solution space with six degrees of freedom, given by the vector: $\mathbf{x} = [\lambda_{CP} \quad n_{FC} \quad n_{BATT} \quad P_{pa} \quad P_{batt} \quad K_{ch}]^T$. A summary of the design variables is provided in Table 1.

<i>Design Variables</i>		
x_1 :	compressor scale	λ_{CP}
x_2 :	number of fuel cells	n_{FC}
x_3 :	number of battery modules	n_{BATT}
x_4 :	threshold power value for power assist mode	P_{pa}
x_5 :	threshold power value for battery only mode	P_{batt}
x_6 :	battery charge control gain	K_{ch}

Table 1: Design Variables

4.3 Constraints

The constraints imposed on the optimization problem consist of practical constraints, engineering goals, and model validity constraints. Initially, all modeling validity constraints will be included to aide the optimization algorithms. However, if any of these constraints become active then the

model must be reassessed and modified. This process will occur during the optimization phase of the project.

All design variables represent physical dimensional quantities or control gains. As such, a positivity constraint is required:

$$\mathbf{x} = [\lambda_{CP} \quad n_{FC} \quad n_{BATT} \quad P_{pa} \quad P_{batt} \quad K_{ch}]^T > \mathbf{0} \quad (12)$$

The next groups of constraints represent limits on each design variable to ensure a well-bounded optimization problem. In some sense, each of these is a model validity constraint. Although they ensure a well-bounded problem, it is not desirable for any of the constraints to become active. This fact is discussed in Section 6.1. These simple bounds are as follows:

$$0.5 \leq \lambda_{CP} \leq 2.0 \quad (13)$$

$$300 \leq n_{FC} \leq 500 \quad (14)$$

$$10 \leq n_{BATT} \leq 50 \quad (15)$$

$$7200W \leq P_{pa} \leq 10,500W \quad (16)$$

$$6500W \leq P_{batt} \leq 8000W \quad (17)$$

$$1 \leq K_{ch} \leq 100 \quad (18)$$

Packaging and scaling assumptions requires simple bounds on the compressor scale ratio. Automotive packaging requirements constrain the number of fuel cells and battery modules. For stationary applications, these constraints would not exist, as weight and packaging is not a concern. The power threshold values for the power assist and battery only modes are selected to bracket the power demand cycle used in this simulation. Note that these values are bounded such that $P_{pa} > P_{batt}$. This choice maintains the integrity of the rule-based control methodology. If violated, the rule-based controller would not operate correctly. Limits on the charge gain, K_{ch} , are chosen arbitrarily.

The remaining constraints consist of the practical constraints, engineering goals, and model validity constraints mentioned previously. For centrifugal and axial compressors, a phenomenon known as surge occurs when the compressor becomes unstable and creates a reversal of flow. This occurs when the pressure ratio exceeds a characteristic value for any given mass flow rate.

Compressor surge will cause massive power loss and damage to the compressor. Several sophisticated anti-surge controllers have been developed in the literature. For simplicity, however, a constraint is applied to ensure the compressor never enters the surge region. This constraint is a linear approximation of the surge line that separates the unstable surge region from the stable region, demonstrated by the dashed line depicted in Figure 8 [2]. If this constraint becomes active for the optimal solution, further investigation is required on compressor design.

$$6.5W_{CP} - 1.05 \leq \frac{P_{SM}}{P_{atm}} \quad (19)$$

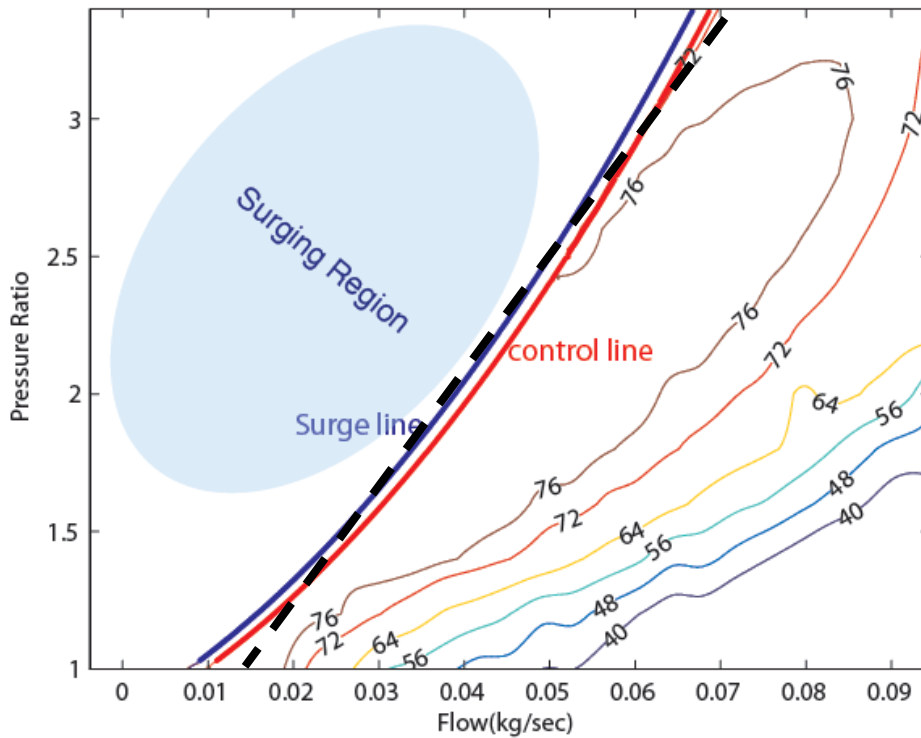


Figure 9: Surge region and the surge line approximation, given by dashed line, on a compressor map [2].

The model assumes a linear nozzle equation for the flow between the supply manifold and cathode, thus requiring a small pressure difference between both components. To ensure this assumption is met, the optimization algorithm must satisfy the constraint given below.

$$\left| \frac{P_{CA}}{P_{SM}} - 1 \right| \leq 0.1 \quad (20)$$

In order to design a fuel cell stack that can be reasonably packaged in an automobile, considerations for physical dimensions are necessary. A typical value for the track width of an

automobile is about 5 ft or 1.5m. Suppose 80% of the total track width is available for fuel cell stack installation, due to packing and safety concerns, thereby constraining the total fuel cell stack length to 1.2m. Also, assume each cell is comprised of the MEA, anode, cathode, backing layers and flow fields, where the backing layers and flow fields account for 50% of the total cell width. This series of assumptions, based on reasonable packing considerations for a commercially available automobile, produce the following constraint:

$$L_{st}(n_{fc}) \leq 1.2m \quad (21)$$

Although a necessary component to any hybrid automobile, batteries are very heavy. Utilizing a high capacity battery will, in general, improve range and mileage. However, high capacity necessitates greater mass, which in general decreases range and mileage. This tradeoff is clear for mobile scenarios. However, weight is not a concern for stationary power. Since the intent of the V2G system is to design a power plant optimal for both applications, a constraint on total battery weight is necessary. Suppose, simply for the purposes of this class project, that the maximum allowable weight for the battery is 75 lbs, thus bounding the number of battery modules from above.

$$M_{batt}(n_{batt}) \leq 75lbs \quad (22)$$

The physical model described in [7] predicts heat dissipated through electrochemical reactions in the fuel cell stack. The amount of heat disappointed is most clearly related to the total number of cells. For a relatively large number of cells, the stack produces more voltage and therefore requires less current to generate the same amount of power for a nominal number of cells. Therefore, limiting the amount of allowable heat generation places a lower bound on the number of cells in the stack. For the sake of developing a constraint pertinent to the optimization problem, assume the amount of heat generated in the stack cannot exceed 7500W.

$$\dot{Q}_{st} \leq 7500W \quad (23)$$

The fuel cell system model assumes all power required by auxiliary components is provided by the stack itself. Clearly, this configuration degrades the overall efficiency of the system, but is typical to vehicle applications without secondary power sources. The relative sizes between the fuel cell stack and compressor must be chosen carefully such that auxiliary component power draw does not dominate overall power consumption. To ensure this condition, it is required that the average ratio of compressor motor power to fuel cell stack power does not exceed 10%.

$$\text{avg} \left(\frac{P_{CM}}{P_{st}} \right) \leq 10\% \quad (24)$$

A critical benefit to fuel cell systems is the relatively high efficiency in comparison to internal combustion engines. Total system efficiency becomes a function of many variables in a hybrid system, such as the one suggested in this report. As such, a design is required that maintains a certain level of efficiency, seen suitable for both vehicle and stationary power. For the sake of argument, suppose the desired fuel cell system efficiency must exceed 60%.

$$\eta_{fc} \geq 60\% \quad (25)$$

Oxygen excess ratio is yet another metric for determining fuel cell system performance. This value is defined as the ratio of oxygen supplied to oxygen used in the cathode. Ensuring proper levels of oxygen in the cathode circumvents reactant starvation and therefore energy efficiency. Past work on fuel cell system modeling has shown that the highest net power is achieved for an oxygen excess ratio between 2 and 2.4 [7], assuming steady-state operation. For our study, we shall impose a more conservative constraint due to the high occurrence of transients. The formulation is given below, which states that the average oxygen excess ratio over the entire response must exist between values of 2 and 3.

$$2 \leq \lambda_{O_2} \leq 2.5 \quad (26)$$

To ensure high efficiency and long battery life, the state of charge (SOC) must be maintained within an optimal operating region, for every time step k . The rule-based control algorithm attempts to maintain a desired SOC, but the actual SOC trajectory can deviate from this value. Therefore, the following limits are imposed on SOC.

$$\max_k \{SOC(k)\} \leq SOC_{\max} \quad (26)$$

$$\min_k \{SOC(k)\} \geq SOC_{\min} \quad (27)$$

An additional constraint is needed to ensure that the SOC level after a complete cycle does not deviate from the initial SOC level by more than certain value, where N is the total number of time steps in the cycle. This necessary constraint ensures the battery never discharges completely or overcharges past its capacity, for a series of cycles.

$$\frac{|SOC(1) - SOC(N)|}{SOC(1)} \leq \Delta SOC_{\max} \quad (28)$$

These constraints represent a preliminary list that will be expanded upon and updated as the project progresses forward.

4.4 Model Parameters

The model parameters include the stack temperature, compressor motor constants, membrane water content, membrane thickness, fuel cell active area, component volumes, return manifold throttle area, orifice constants, maximum SOC, maximum change of SOC, and maximum power request. Although this list is quite comprehensive, it only represents the most significant parameters. The values for each parameter described are given in Table 2.

<i>Symbol</i>	<i>Parameter</i>	<i>Value</i>
κ_t	Motor Parameter	0.0153 N·m/A
T_{ST}	Stack Temperature	80° C
λ_m	Membrane Water Content	14
t_m	Membrane Thickness	0.01275 cm
A_{FC}	Fuel Cell Active Area	280 cm ²
V_{AN}	Anode Volume	0.005 m ³
V_{CA}	Cathode Volume	0.01 m ³
V_{SM}	Supply Manifold Volume	0.02 m ³
V_{RM}	Return Manifold Volume	0.005 m ³
$A_{T, RM}$	Return Manifold Throttle Area	0.002 m ²
$\kappa_{SM, OUT}$	Supply Manifold Outlet Orifice Constant	$0.3629 \times 10^{-5} \text{ kg}/(\text{s} \cdot \text{Pa})$
$\kappa_{CA, OUT}$	Cathode Outlet Orifice Constant	$0.2177 \times 10^{-5} \text{ kg}/(\text{s} \cdot \text{Pa})$
SOC_{min}	Minimum Allowable State of Charge	0.6
SOC_{max}	Maximum Allowable State of Charge	0.75
ΔSOC_{max}	Maximum Change in SOC at End of Cycle	0.01

Table 2: Model Parameters

4.5 Optimization Problem Summary

The following system of equations and inequalities summarizes the optimization problem in negative null form.

$$\begin{aligned}
 & \text{minimize} && f(\mathbf{x}) = m_{H_2}(\lambda_{CP}, n_{FC}, n_{BATT}, P_{pa}, P_{batt}, K_{ch}) \\
 & \text{with respect to} && \mathbf{x} = [\lambda_{CP} \quad n_{FC} \quad n_{BATT} \quad P_{pa} \quad P_{batt} \quad K_{ch}]^T \\
 & \text{subject to} && \mathbf{x} = [\lambda_{CP} \quad n_{FC} \quad n_{BATT} \quad P_{pa} \quad P_{batt} \quad K_{ch}]^T > \mathbf{0}
 \end{aligned}$$

$$\begin{aligned}
 g_1 : \quad & 0.5 - \lambda_{CP} \leq 0 & g_{13} : \quad & 6.5W_{CP}P_{atm} - 1.05p_{atm} - p_{SM} \leq 0 \\
 g_2 : \quad & \lambda_{CP} - 2.0 \leq 0 & g_{14} : \quad & 0.9p_{SM} - p_{CA} \leq 0 \\
 g_3 : \quad & 300 - n_{FC} \leq 0 & g_{15} : \quad & p_{CA} - 1.1p_{SM} \leq 0 \\
 g_4 : \quad & n_{FC} - 500 \leq 0 & g_{16} : \quad & L_{st}(n_{fc}) - 1.2 \leq 0 \\
 g_5 : \quad & 10 - n_{BATT} \leq 0 & g_{17} : \quad & m_{batt}(n_{batt}) \cdot g - 75 \leq 0 \\
 g_6 : \quad & n_{BATT} - 50 \leq 0 & g_{18} : \quad & \dot{Q}_{st} - 7500 \leq 0 \\
 g_7 : \quad & 8500 - P_{pa} \leq 0 & g_{19} : \quad & avg\left(\frac{P_{CM}}{P_{st}}\right) - 0.1 \leq 0 \\
 g_8 : \quad & P_{pa} - 10,500 \leq 0 & g_{20} : \quad & 0.6 - \eta_{fc} \leq 0 \\
 g_9 : \quad & 6400 - P_{batt} \leq 0 & g_{21} : \quad & 2 - \lambda_{O_2} \leq 0 \\
 g_{10} : \quad & P_{batt} - 7400 \leq 0 & g_{22} : \quad & \lambda_{O_2} - 2.5 \leq 0 \\
 g_{11} : \quad & 1 - K_{ch} \leq 0 & g_{23} : \quad & \max_k \{SOC(k)\} - SOC_{max} \leq 0 \\
 g_{12} : \quad & K_{ch} - 100 \leq 0 & g_{24} : \quad & SOC_{min} - \min_k \{SOC(k)\} \leq 0 \\
 & & g_{25} : \quad & \frac{|SOC(1) - SOC(N)|}{SOC(1)} - \Delta SOC_{max} \leq 0
 \end{aligned}
 \tag{29}$$

5. Model Analysis

Prior to applying optimization techniques to the problem summarized by Equation (29), a pre-optimality analysis is performed on the model in order to gain a better understanding of the system under study. A discussion on dynamic simulation of the fuel cell system model is presented to expose significant dynamic characteristics and responses for varying inputs. To investigate the design problem at hand, response surfaces for the H₂ fuel consumption and minimum SOC are analyzed with respect to varying design variables. From this study, the monotonic properties of several design variables are determined, consequently enabling the use of a “pseudo” monotonicity analysis. Due to the nature of the problem at hand, analysis performed through simulation produces noisy responses. This presents an interesting problem for a derivative-based optimization algorithm which, in general, requires continuous and smooth responses. The solution proposed in this work is to develop a surrogate model using neural networks.

5.1 Dynamic Simulation

To understand the characteristics of a dynamic fuel cell system model, a series of step changes in stack current is applied as an input, shown in Figure 10(a). A static feedforward controller uses the current input plus some first order dynamics to determine the appropriate compressor motor input voltage, a shown in Figure 10(d). This compressor motor voltage drives the lumped inertial mass of the compressor and motor according to the response given by Figure 10(e). For a positive step in input current, the stack voltage initially drops (Figure 10(b)) due to the temporary depletion of oxygen in the cathode (Figure 10(f)). As the inner loop controller attempts to regulate the oxygen excess ratio to a value of two, the stack voltage reaches steady state. The product of stack voltage and current produces the stack power illustrated in Figure 10(c). The compressor motor consumes a percentage of stack power and the resulting net power is also given in Figure 10(c).

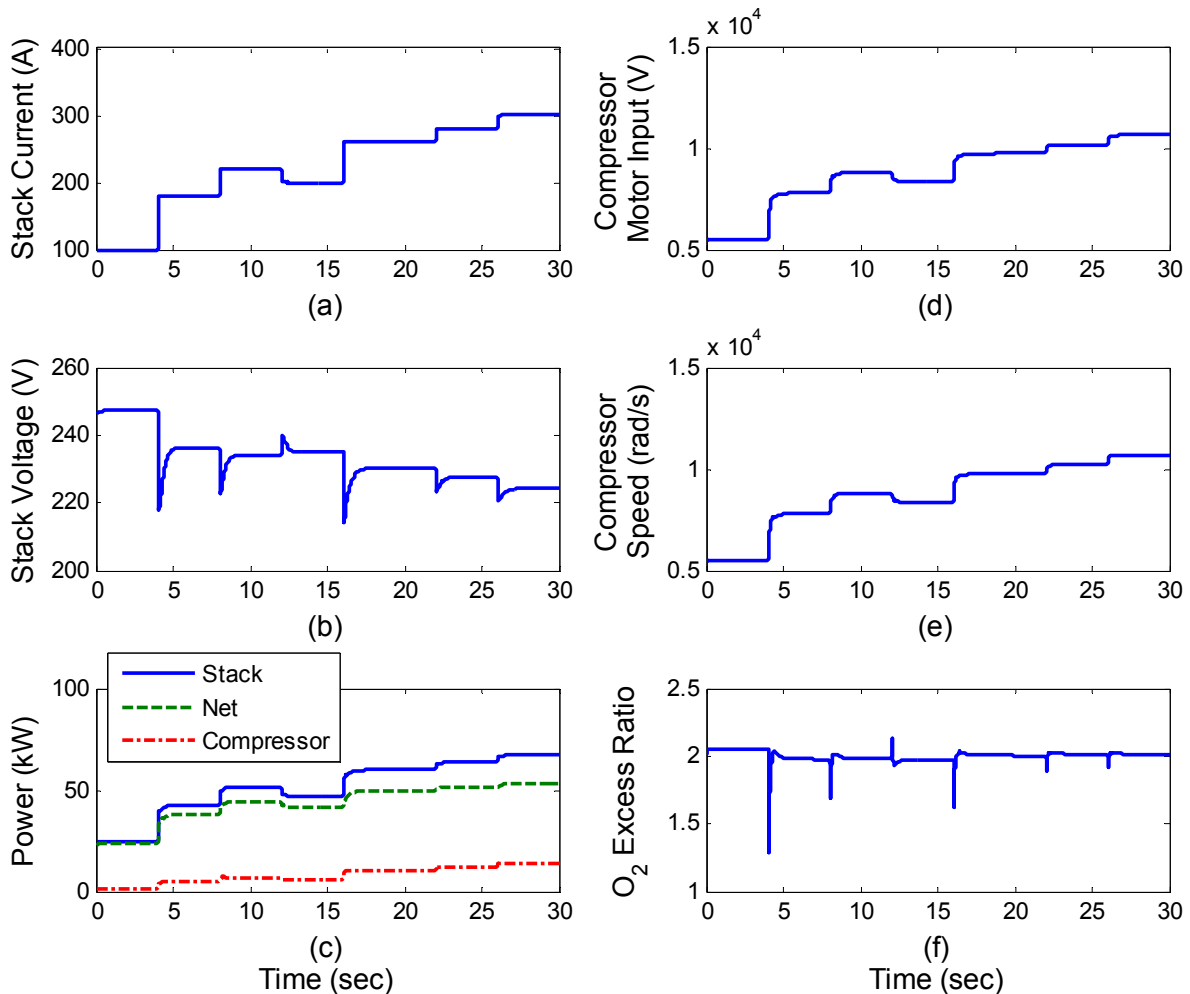


Figure 10: Dynamic simulation responses for a series of current input step changes, shown in (a).

Overall, the fuel cell system model developed by Pukrushpan contains a total of nine states [7]. However, the step responses shown in Figure 10 closely mimic a much simpler first-order dynamic system with very fast settling time. If one desired to reduce simulation time, which was not an issue in our case, then the nine state dynamic system could be reduced to a single state dynamic system with steady-state input/output mapping. This technique was successfully used in a similar study by Han [2].

5.2 Design of Experiments Study

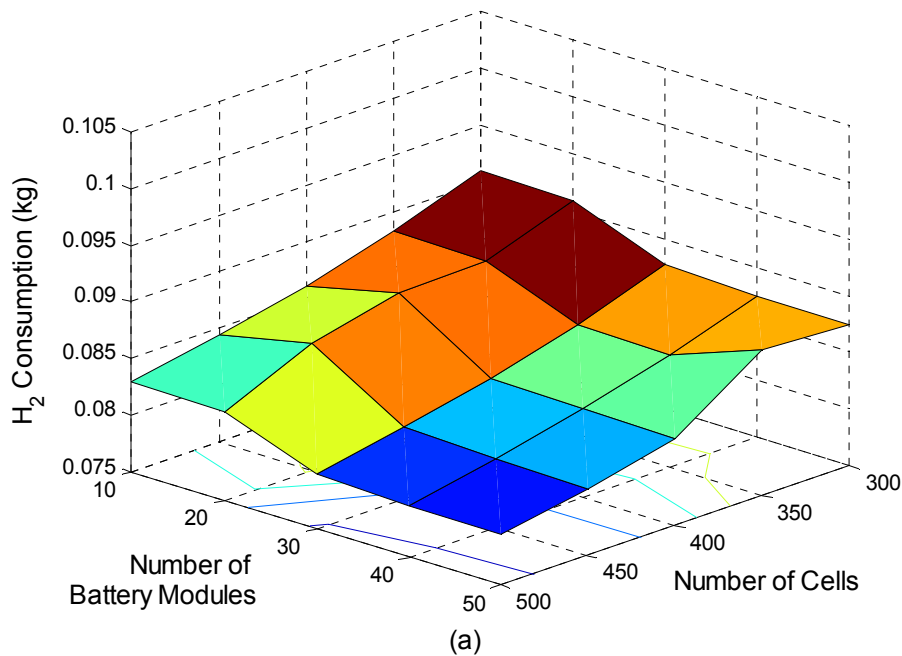
The system response varies with changes in values for the design variables described in Section 4.2. How this variation occurs is initially unclear, therefore motivating the need for optimization techniques. However, it is often desirable to get a preliminary understanding of how the objective and constraint functions react to varying each design variable. To aid this effort, the surface plots in Figures 9 and 10 were developed to demonstrate how the model reacts to varying two variables at a time, while leaving the remaining four at constant nominal values. These nominal values are given by Table 3. Note that these surfaces only represent two-dimensional slices through a six-dimensional design space. As a result, conclusions regarding these surfaces cannot be extrapolated to the entire design space.

<i>Design Variable</i>	<i>Nominal Value</i>
Number of Fuel Cells in Stack, n_{FC}	400
Number of Battery Modules, n_{BATT}	30
Compressor Scale, λ_{CP}	10
Power Assist Mode Threshold, P_{pa}	6850 W
Battery Only Mode Threshold, P_{batt}	9250 W
Charge Gain, K_{ch}	10

Table 3: For the response surface shown in Figure 11, two variables are adjusted while the remaining four are fixed at the nominal values shown here.

Several significant observations are made by analyzing Figure 11. (1) H₂ fuel consumption appears to be most sensitive to changes in the power threshold, values and least sensitive to the number of cells and battery modules. This observation elucidates the importance of control design to the performance of the system and predicates one of the key conclusions to this work. A successful engineering design can often be found by using smaller, more efficient component

sizes with a well designed control scheme. (2) For the design space cross sections shown, the objective is very clearly monotonic with respect to both power mode threshold values. The general trend indicates that selected modes which limit the “fuel cell only” mode and maximize battery participation provide the highest fuel economy. In the case of compressor scale, there exists regional monotonicity, in which it can be seen the minimum objective function value occurs for minimum compressor size, $\lambda_{cp} = 0.5$. Therefore, it may be predicted that the optimal solution includes power thresholds that minimize the “fuel cell only” region and compressor scale. (3) Multiple local minima may exist, as indicated by the undulating surfaces in Figure 11. In particular, the number of cells, battery modules, and charge gain are characterized as wavy, signifying that these variables may contain interior optima. However, if the wavy characteristic is ignored, it becomes clear that fuel consumption decreases as the number of cells and battery modules increases. Hence, there must exist active constraints which bound these two variables from above. (4) Both power assist and battery only mode threshold values are highly coupled. This fact is easily seen in Figure 11(b) because the response surface is characterized by a three-dimensional shape, as opposed to Figures 11(a) and (c) which appear to be nearly two-dimensional or constant with respect to one of the variables.



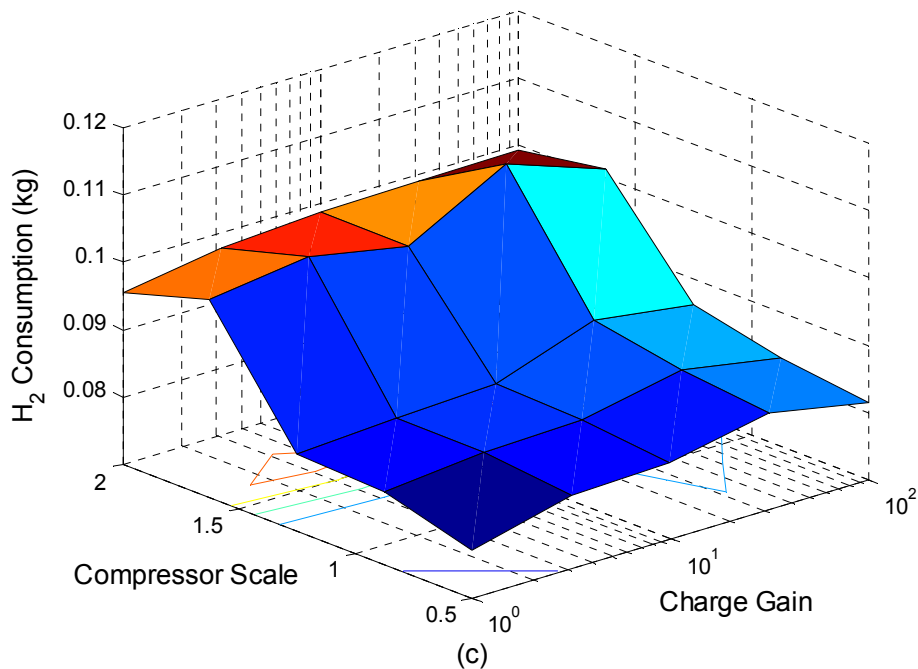
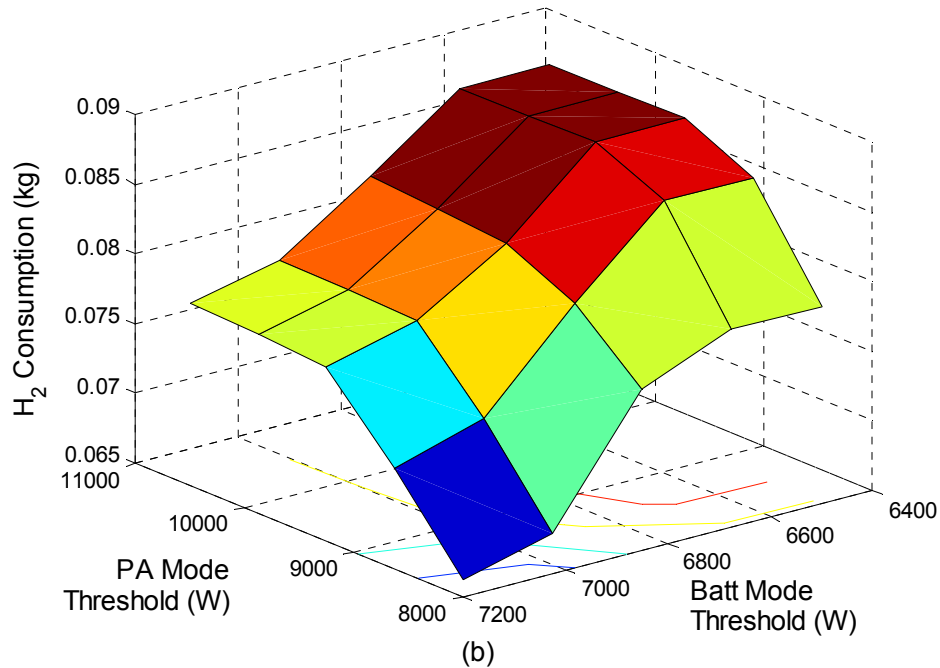


Figure 11: Response surface of H₂ consumption with respect to varying two design variables at once. The remaining four variables are set to constant nominal values.

A similar analysis is shown here for the response of minimum SOC. This constraint is of particular interest because it potentially may constrain four different design variables: PA mode threshold, battery mode threshold, number of battery modules, and charge gain. As a result, identifying monotonic relationships may be particularly useful determining if this constraint

becomes active. Figure 12(a) suggests that the minimum SOC decreases as battery mode increases. Therefore, the battery mode threshold may be bounded above by this constraint. Figure 12(b) indicates minimum SOC increases as both the number of battery modules and charge gain increase, implying those variables are bounded from below by this constraint. The observations made here shall be invoked in the monotonicity analysis given in the following section.

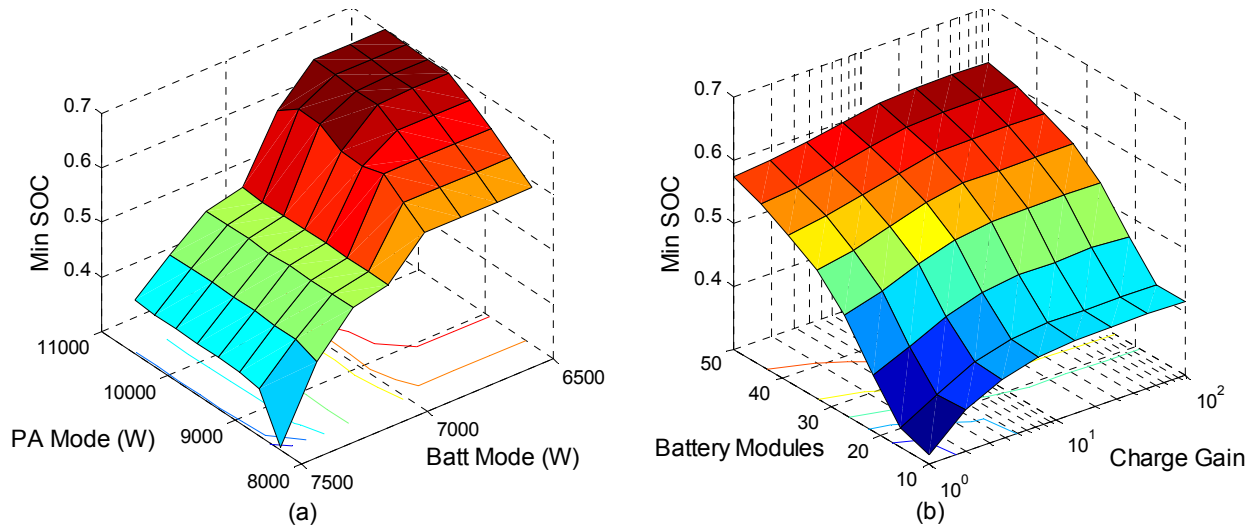


Figure 12: Response surface of minimum SOC with respect to varying two design variables at once. The remaining four variables are set to constant nominal values.

Although it is tempting to apply monotonicity analysis using observations from Figures 11 and 12, it would be inappropriate because these surfaces are two-dimensional subspaces of a much more complex six-dimensional space. Nevertheless, the study of each response surface provides a useful internal understanding of the design optimization problem under investigation.

5.3 Monotonicity Analysis

Monotonic analysis is an extremely powerful tool for solving optimization problems by way of determining monotonic relationships between each variable and the objective function. In general, this analysis is applicable to analytic systems in which determining monotonic relationships is easily done through simple algebra and calculus operations. Since the model presented in this work is a strict numerical simulation, performing such analysis is not easily done in such a rigorous manner. However, a simple investigation of planar response surfaces through the six-dimensional design space allows us to predict monotonic relationships. The

result is a reduction of the original optimization problem formulation and prediction of the actual solution.

From Figure 11, it is possible to observe monotonic properties of the objective function with respect to certain design variables. For example, as the number of fuel cells and battery mode threshold increase, the total fuel consumed decreases monotonically. As the PA mode threshold increases, the total fuel consumed increases monotonically. Compressor scale exhibits regional monotonicity, in which the total fuel consumed increases as compressor scale increases up to about 1.625. Conversely, fuel consumption decreases as compressor scale increases above 1.625.

Assuming these trends persist throughout the design space, observing the monotonicity of various constraints may provide an indication of the solution. A monotonicity table is given in Table 4, including several constraints which we suspect may become active at the solution. Specifically, it is predicted that constraints on maximum fuel cell stack length, maximum battery weight, average parasitic loss, and minimum SOC will become active constraints at the optimum. In the case of fuel cell stack length and battery weight, these constraints are functions of single variables, the number of fuel cells and battery modules, respectively. Assuming these constraints are not dominated by any others, the optimal solution for number of fuel cells and battery modules is 421 and 34, correspondingly.

		n_{FC}	n_{BATT}	λ_{CP}	P_{pa}	P_{batt}	K_{ch}	Suspected Activity
Fuel consumption	$f(\mathbf{x})$	-	-	+ or -	+	-	?	N/A
Fuel Cell Stack Length	g_{16}	+						ACTIVE by MP1 wrt n_{FC}
Battery weight	g_{17}		+					ACTIVE by MP1 wrt n_{BATT}
Minimum SOC	g_{23}	?	-	?	?	+	-	ACTIVE by MP1 wrt <u>at least one</u> variable

Table 4: Monotonicity table for objective and three active constraint functions

5.4 Surrogate Modeling through Neural Networks

Neural networks offer an elegant methodology for modeling complex systems using an input-output approach. It is a common strategy for approximating complex multi-dimensional functions, and therefore well-suited for surrogate modeling. Most importantly, neural networks produce continuous, smooth functions using drastically less computational power than simulating the full system. The clear tradeoff, however, is that a neural network fabricates an approximation of the system response. The accuracy of each approximation scales with how much data is used to train the network. The training data must be obtained from the actual system simulation. Therefore, a balance must be struck between computational cost associated with obtaining training data and accuracy desired for function approximation.

A radial basis network is selected for function fitting due to its fast training time relative to feed forward networks. The input vector is formed by meshing the design space such that each variable has five nodes. For six design variables, this results in a total of $5^6 = 15625$ nodes, therefore requiring 15625 separate simulations. The resulting objective and constraint values for each simulation are stored to produce target vectors. Simulating 15625 responses at about 1.7 seconds per simulation on a CAEN computing workstation requires 7 hours and 22 minutes, which is a reasonable overnight simulation time, barring any errors. However, to speed up the computation process, five computers were coordinated to operate simultaneously and the resulting data was consolidated.

Two types of neural networks are analyzed to form the most suitable surrogate model of the fuel cell hybrid system. First, a standard two-layer feed-forward neural network (FFNN) is trained with the Levenberg-Marquardt algorithm, a quasi-Newton optimization techniques that uses Hessian approximation to achieve near quadratic convergence speed. The second method employs generalized regression neural networks (GRNN), which contains a radial basis layer and special linear layer. Since the topic of neural networks exists outside the scope of the course, a detailed discussion is omitted. Instead, both approximation methods are compared and it is decided the FFNN method offers the most accurate approximation of the system response, for both the objective and constraint function values. To illustrate this result, Figure 13 provides

representative plots of both neural network approximations in relation to the actual simulation values. In each plot, a single design variable is adjusted while fixing the remaining five to the nominal values. From Figure 13, it is clear both neural network techniques do a reasonably good job of approximating the simulated values. However, it is also evident that neural network approximations only capture overall trends and may overlook local optima. For example, consider the design represented in Figure 13(a) with 438 cells. This design consumes 0.07921 kg of H₂, the minimum for all feasible values of n_{FC} . However, the neural networks predict 500 cells as the minimizer, thus highlighting the inherent disadvantage of surrogate modeling.

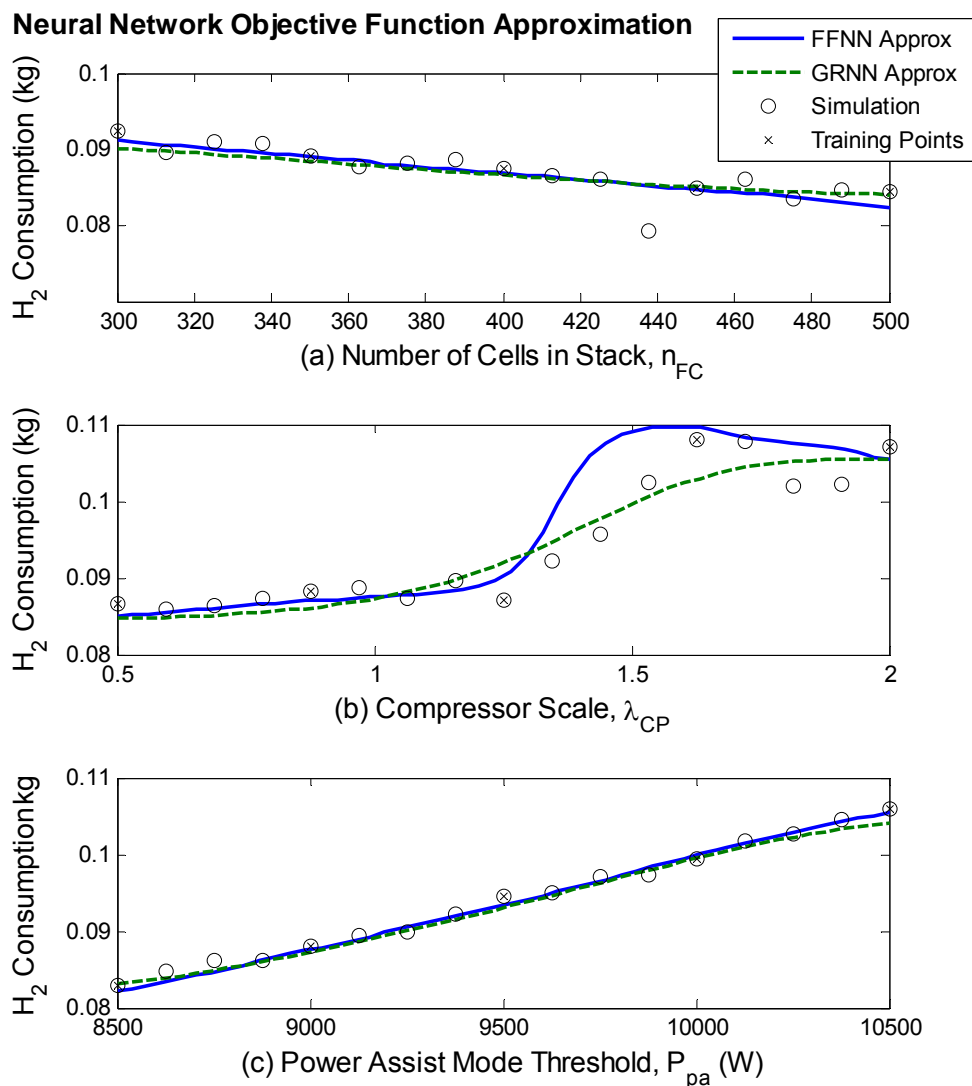


Figure 13: Neural network objective function approximations wrt to the (a) number of cells in the stack, (b) compressor scale, and (c) power assist mode threshold value. The true values are denoted by circles, while the x's denote points used for training each neural network.

6. Optimization Study

A sequential quadratic programming (SQP) method is utilized to optimize the problem formulated in Section 4. The application of a gradient based algorithm is enabled creating a continuous and differential surrogate model through neural networks. This methodology offers clear advantages in terms of analysis, since a variety of tools are available for gradient based algorithms. Several issues are discussed, including constraint activity, the role of Lagrange multiplier values, interior vs. boundary solutions, global and local results, numerical stability, satisfaction of the Karush-Kuhn-Tucker (KKT) conditions, and varying starting points. In total, the analysis provides critical inside to the nature of the optimal solution.

6.1 Optimization Results

In the case of SQP, the algorithm solves a quadratic programming (QP) sub-problem using an active set strategy at each iteration. The Hessian of the Lagrangian is estimated using the BFGS formula and line search is performed via merit functions to ensure feasibility and descent [10]. The application of this algorithm to the surrogate model generates the resulting optimal solution, given in Table 5.

<i>Design Variable</i>	<i>Optimal Value</i>
Number of Fuel Cells in Stack, n_{FC}	422
Number of Battery Modules, n_{BATT}	32
Compressor Scale, λ_{CP}	0.5
Power Assist Mode Threshold, P_{pa}	8074 W
Battery Only Mode Threshold, P_{batt}	6662 W
Charge Gain, K_{ch}	1.412
H_2 Fuel Consumption, m_{H_2}	0.0756 kg

Table 5: Solution to the optimization problem as found by SQP.

Preliminary observations of the optimal solution reveal several important trends. (1) The compressor tends to its smallest possible size, partially to alleviate auxiliary power drain from the stack. This result is reasonably expected, since Figure 13(b) indicated a general trend of decreasing fuel consumption for decreasing compressor scale, using nominal values for the remaining design variables. (2) Solutions at the boundaries of the surrogate model represent active model validity constraints. This is an issue because the limitations of our surrogate modeling bounded the solution, therefore requiring further investigation into proper function

approximation using neural networks. This result is a clear drawback, but does not limit the ability to find design solutions using the original simulation model. (3) The number of fuel cells and battery modules approach the limit given by the stack length and battery weight constraints, respectively. The “pseudo” monotonicity analysis predicted this result, therefore validating the assumptions previously made about extending monotonic relations for a two-dimensional subspace of the six-dimensional design space.

6.2 Constraint Activity

In total, the optimization problem contains 25 inequality constraints, which include both engineering and model validity constraints. As discussed previously, special care is taken for active model validity constraints, within the context of optimizing using the surrogate model.

	<i>Constraint</i>	<i>Activity</i>
λ_{CP} lower bound	$g_1 : 0.5 - \lambda_{CP} \leq 0$	ACTIVE
λ_{CP} upper bound	$g_2 : \lambda_{CP} - 2.0 \leq 0$	INACTIVE
n_{FC} lower bound	$g_3 : 300 - n_{FC} \leq 0$	INACTIVE
n_{FC} upper bound	$g_4 : n_{FC} - 500 \leq 0$	INACTIVE
n_{BATT} lower bound	$g_5 : 10 - n_{BATT} \leq 0$	INACTIVE
n_{BATT} upper bound	$g_6 : n_{BATT} - 50 \leq 0$	INACTIVE
P_{pa} lower bound	$g_7 : 7200 - P_{pa} \leq 0$	INACTIVE
P_{pa} upper bound	$g_8 : P_{pa} - 10,500 \leq 0$	INACTIVE
P_{batt} lower bound	$g_9 : 6500 - P_{batt} \leq 0$	INACTIVE
P_{batt} upper bound	$g_{10} : P_{batt} - 8000 \leq 0$	INACTIVE
K_{ch} lower bound	$g_{11} : 1 - K_{ch} \leq 0$	INACTIVE
K_{ch} upper bound	$g_{12} : K_{ch} - 100 \leq 0$	INACTIVE
Compressor surge	$g_{13} : 6.5W_{CP}p_{atm} - 1.05p_{atm} - p_{SM} \leq 0$	INACTIVE
SM Linear Nozzle Assumption	$g_{14} : 0.9p_{SM} - p_{CA} \leq 0$	INACTIVE
SM Linear Nozzle Assumption	$g_{15} : p_{CA} - 1.1p_{SM} \leq 0$	INACTIVE
Fuel cell stack length	$g_{16} : L_{st}(n_{fc}) - 1.2 \leq 0$	ACTIVE
Battery weight	$g_{17} : m_{batt}(n_{batt}) \cdot g - 75 \leq 0$	ACTIVE
Stack heat generation	$g_{18} : \dot{Q}_{st} - 7500 \leq 0$	INACTIVE
Average parasitic loss	$g_{19} : avg\left(\frac{P_{CM}}{P_{st}}\right) - 0.1 \leq 0$	INACTIVE
Fuel cell system efficiency	$g_{20} : 0.6 - \eta_{fc} \leq 0$	INACTIVE

Oxygen Excess Ratio	$g_{21} : 2 - \lambda_{O_2} \leq 0$	INACTIVE
Oxygen Excess Ratio	$g_{22} : \lambda_{O_2} - 2.5 \leq 0$	INACTIVE
Maximum SOC	$g_{23} : \max_k \{SOC(k)\} - SOC_{\max} \leq 0$	INACTIVE
Minimum SOC	$g_{24} : SOC_{\min} - \min_k \{SOC(k)\} \leq 0$	ACTIVE
Maximum SOC displacement	$g_{25} : \frac{ SOC(1) - SOC(N) }{SOC(1)} - \Delta SOC_{\max} \leq 0$	INACTIVE

Table 6: Constraint activity

The active constraint given by g_1 is a model validity constraint. Even though the claim cannot be made that this constraints defines the optimal solution, they provide important insight to the nature of the true solution. In the case of g_1 , activity indicates the smallest feasible compressor scale results in the lowest fuel consumption. This is reasoned by the fact that a larger compressor consumes more power, which degrades system efficiency. However, preliminary model analysis has shown that the limit on oxygen excess ratio does in fact provide a lower bound on the compressor size. This behavior is lost in the transition to a surrogate model, thus enabling compressor scale to decrease to the lower bound.

Constraints g_{16} and g_{17} bound the number of cells, n_{FC} , and number of battery modules, n_{BATT} , respectively, from above. As a result, the optimal hybrid fuel cell system component sizes are characterized by the longest fuel cell stack and heaviest battery that is feasibly possible. For stationary applications, packing and weight is usually not an issue of concern. However, these two issues are paramount to vehicle system design. The parametric study given in the subsequent section expands on this idea by reformulating these constraints as part of the objective, thus creating a multi-objective optimization problem. From that point, Pareto optima are analyzed to trade offs with respect to the relative importance of each objective.

In addition to the constraints bounding component sizes, minimum SOC becomes active at the solution. Intuition suggested this constraint is active at the optimum, as argued by monotonicity analysis. This constraint also represents a key tradeoff that exists in the problem. The objective function decreases when battery participation is maximized. However, this clearly degrades SOC, which the designer hopes to maintain at relatively constant levels to ensure maximum

battery life. The result shown here confirms the argument given above, suggesting that minimal fuel consumption is achieved for a design that sacrifices the most allowable charge depreciation.

6.3 Lagrange Multipliers

Lagrange multipliers are rich with information regarding the nature of the solution through post-optimality analysis. At the local constrained minimum, given by x_* , the solution satisfies the necessary optimality conditions known as Karush-Kuhn-Tucker (KKT) conditions. In its most general form, these conditions are given by Equation (30) [10]. For the problem under consideration, no equality constraints, given by $\mathbf{h}(\mathbf{x})$, exist, so λ may be disregarded.

$$\begin{aligned}
 \text{Stationarity: } & \nabla f_* + \lambda^T \nabla \mathbf{h}_* + \boldsymbol{\mu}^T \nabla \mathbf{g}_* = \mathbf{0}^T \\
 \text{Feasibility: } & \mathbf{h}(\mathbf{x}_*) = \mathbf{0}, \mathbf{g}(\mathbf{x}_*) \leq \mathbf{0} \\
 \text{Transversality: } & \boldsymbol{\mu}^T \mathbf{g} = 0 \\
 \text{Multipliers: } & \lambda \neq \mathbf{0}, \boldsymbol{\mu} \geq \mathbf{0}
 \end{aligned} \tag{30}$$

A nonzero value for the Lagrange multiplier, $\boldsymbol{\mu}$, indicates activity on the corresponding inequality constraint. Table 7 provides the values of each Lagrange multiplier for the active inequality constraints. Inactive inequality constraints have multiplier values of zero and are thus inconsequential to the solution.

<i>Active Constraints</i>		<i>Lagrange Multiplier Values, $\boldsymbol{\mu}$, at Optimum</i>
λ_{CP} lower bound	$g_1 : 0.5 - \lambda_{CP} \leq 0$	3.857
Fuel cell stack length	$g_{16} : L_{st}(n_{fc}) - 1.2 \leq 0$	9.551
Battery weight	$g_{17} : m_{batt}(n_{batt}) \cdot g - 75 \leq 0$	19.549
Minimum SOC	$g_{24} : SOC_{\min} - \min_k \{SOC(k)\} \leq 0$	53.102

Table 7: Lagrange multiplier values at the optimum for active constraints.

Besides indicating activity, the multiplier values themselves are related to how sensitive the objective function is with respect to changes in the constraint function values according to

$$\left(\frac{\partial f}{\partial \mathbf{h}} \right)_* = -\lambda^T \tag{31}$$

where $(\partial f / \partial \mathbf{h})_*$ is the change in the objective function with respect to changes in the constraint functions at the optimum. Equation (31) is valid for only small changes, since this derivation is based on a first-order approximation near \mathbf{x}_* . After normalizing the constraint function values, Table 7 indicates that the solution is most sensitive to the minimum state of charge constraint.

Since g_{24} potentially bounds any of the six design variables, it is hypothesized that this constraint is the most constrictive to the optimal solution. To illustrate this fact, suppose g_{24} is relaxed such that the minimum allowable state of charge during the response is 0.5. The resulting optimal design consumes 0.072777 kg, an improvement of 2.62%. Moreover, the active constraints now include stack length, battery weight, SOC displacement, and lower bounds on λ_{CP} , P_{pa} , K_{ch} . For this relaxed solution, the constraint with the greatest sensitivity is the lower bound on power assist mode threshold. Therefore, it is argued that this constraint is the second most constrictive for the surrogate model, near the solution. However, it is more interesting to note that a new constraint becomes active during the constraint relaxation analysis, maximum SOC displacement. This result indicates that the minimum SOC constraint dominates maximum SOC displacement, near the solution. This result is analyzed further during the parametric analysis given in a subsequent section. All of these results are summarized by Table 8.

<i>Design Variable</i>	<i>Optimal Value for Relaxed Problem</i>
Number of Fuel Cells in Stack, n_{FC}	423
Number of Battery Modules, n_{BATT}	32
Compressor Scale, λ_{CP}	0.5
Power Assist Mode Threshold, P_{pa}	8000 W
Battery Only Mode Threshold, P_{batt}	6708 W
Charge Gain, K_{ch}	1
H ₂ Fuel Consumption, m_{H_2}	0.077277 kg

(a)

	<i>Active Constraints</i>	<i>Lagrange Multiplier Values, μ, at Optimum</i>
λ_{CP} lower bound	$g_1 : 0.5 - \lambda_{CP} \leq 0$	2.6485
P_{pa} lower bound	$g_7 : 8000 - P_{pa} \leq 0$	20.4713
K_{ch} lower bound	$g_{11} : 1 - K_{ch} \leq 0$	0.1495
Fuel cell stack length	$g_{16} : L_{st}(n_{fc}) - 1.2 \leq 0$	6.0449
Battery weight	$g_{17} : m_{batt}(n_{batt}) \cdot g - 75 \leq 0$	1.3036
Maximum SOC displacement	$g_{25} : \frac{ SOC(1) - SOC(N) }{SOC(1)} - \Delta SOC_{max} \leq 0$	0.5491

(b)

Table 8: Constraint sensitivity analysis: (a) optimal solution without the most constrictive constraint included, (b) Lagrange multiplier values for the relaxed problem.

6.4 Interior vs. Boundary Solutions

Solutions fall into two categories: interior and boundary solutions. An interior optimum indicates the solution is unconstrained, whereas a boundary optimum corresponds to a constrained solution. In order to determine if any of the variables is an interior solution, the necessary first-order optimality condition for an unconstrained problem must be satisfied. This condition is given by a vanishing gradient at the solution [10].

$$\nabla f(\mathbf{x})_* = \mathbf{0}^T \quad (32)$$

The gradient of the objective function for the solution given in Table 5 is

$$\nabla f(\mathbf{x}_*) = [-1.3782 \quad 0.0176 \quad 1.6369 \quad 20.1038 \quad -5.7187 \quad 0.1827] \quad (33)$$

where no element is equal to zero. As a result, it is concluded that all variables are bounded solutions. This result is readily understood prior to analyzing the unconstrained first-order necessary optimality condition because six inequality constraints are active at the solution. For six design variables and six active constraints, the degree of freedom is zero and no interior solutions exist.

The next logical proposition to test is which variable is most likely to be an interior solution, if the constraints are relaxed. If minimizers exist within the exclusive set defined by the bounds for that variable, the design space is characterized by convexity with respect to each of those

variables and they are interior solutions. To illustrate, supposed all of the engineering constraints are removed and the bounds are retained. The resultant solution to the unconstrained (but simply bounded) problem is given in Table 9, along with the gradient of the objective function with respect to each variable x_i . For this problem, SQP is performed using the optimal solution in Table 5 as the initial point. Note that two of the gradient components equal zero, corresponding to n_{BATT} and K_{ch} .

This discovery reveals interesting physical insight to the design of a hybrid fuel cell system for V2G applications. (1) Generally, it is desired to maximize battery power output to offset fuel consumption by the fuel cell. Intuition easily suggests a large battery is well-suited to this task. However, if the fuel cell is required to maintain SOC, a larger battery requires more power from the fuel cell for regulation. This inherent tradeoff is reflected by an interior optimum on the number of battery modules. (2) The charge gain, K_{ch} , can be physically interpreted as how quickly the fuel cell recharges the battery. Similar to the previous point, a high gain ensures excellent SOC regulation and thus greater load on the battery. However, a higher gain sacrifices fast rise time with high control action, requiring more H_2 fuel. The balance of power control between the two energy sources attains an optimal solution when charge gain is equal to 1.9889.

<i>Design Variable</i>	\mathbf{x}_*	$(\partial f / \partial x_i)_*$
Number of Fuel Cells in Stack, n_{FC}	500	-0.5887
Number of Battery Modules, n_{BATT}	40	0
Compressor Scale, λ_{CP}	0.5	0.6827
Power Assist Mode Threshold, P_{pa}	8000 W	9.3337
Battery Only Mode Threshold, P_{batt}	7200 W	-1.5130
Charge Gain, K_{ch}	1.9889	0
H_2 Fuel Consumption, m_{H_2}	0.0611 kg	-

Table 9: Solution to the unconstrained (but simply bounded) optimization problem, with gradient components, using optimal solution from Table 5 as the starting point.

After an exhaustive search of the design space, another interior optimum is found for the unconstrained (but simply bounded) problem when different starting points are used. A starting point with charge gain greater than 6 to 8, depending on the other variables, will produce the solution given in Table 10 where n_{BATT} the only interior minimizer. It is interesting to observe

that both solutions attain the exact same fuel consumption, which suggests they are both global minima. For the unconstrained problem, it appears that the design space can be divided into two subspaces, where starting with each subspace results in a corresponding optimal solution. Further analysis on the variation of initial points for the constrained case is discussed in the subsequent section.

<i>Design Variable</i>	\mathbf{x}_*	$(\partial f / \partial x_i)_*$
Number of Fuel Cells in Stack, n_{FC}	500	-0.5765
Number of Battery Modules, n_{BATT}	40	0
Compressor Scale, λ_{CP}	0.5	0.6771
Power Assist Mode Threshold, P_{pa}	8000 W	9.3039
Battery Only Mode Threshold, P_{batt}	7200 W	-1.4693
Charge Gain, K_{ch}	100	-0.2407
H ₂ Fuel Consumption, m_{H_2}	0.0611 kg	-

Table 10: Solution to the unconstrained (but simply bounded) optimization problem, with gradient components, using a charge gain of 10 as the starting point.

6.5 Variation of Starting Points

As we already discovered in previous sections, varying the initial point for an optimization algorithm may lead to varying local minima. It is therefore necessary to investigate this behavior for our problem formulation. As shown in Equation (34), five different initial points are arbitrarily chosen to find different constrained local minima.

$$\begin{aligned}
 \mathbf{x}_0 &= [n_{FC} \quad n_{BATT} \quad \lambda_{CP} \quad P_{pa} \quad P_{batt} \quad K_{ch}] \\
 \mathbf{x}_{0_1} &= [419 \quad 32 \quad 0.5 \quad 9500 \quad 6800 \quad 100] \\
 \mathbf{x}_{0_2} &= [400 \quad 32 \quad 0.75 \quad 9500 \quad 6500 \quad 10] \\
 \mathbf{x}_{0_3} &= [350 \quad 30 \quad 0.75 \quad 8500 \quad 7000 \quad 10] \\
 \mathbf{x}_{0_4} &= [450 \quad 35 \quad 0.75 \quad 8500 \quad 7000 \quad 10] \\
 \mathbf{x}_{0_5} &= [450 \quad 40 \quad 0.75 \quad 8200 \quad 7000 \quad 10]
 \end{aligned} \tag{34}$$

	Initial condition	\mathbf{x}_{0_1}	\mathbf{x}_{0_2}	\mathbf{x}_{0_3}	\mathbf{x}_{0_4}	\mathbf{x}_{0_5}
x_*	n_{FC}	403.03	403	403	335.76	421.76
	n_{BATT}	32.153	32.15	32.15	32.16	31.759
	λ_{CP}	0.5	0.5	0.5	0.5	0.5
	P_{pa}	8984	8985	8985	8000	8074
	P_{batt}	6780	6779	6779	6669	6662
	K_{ch}	1	1	1	1.4386	1.412
$f(x_*) = m_{H_2}$	surrogate	0.07933	0.07936	0.07936	0.07582	0.0751
	simulation	0.0818	0.0817	0.0817	0.0770	0.0756
Constraints	FC length	Active	Active	Active	Inactive	Active
	Battery weight	Active	Active	Active	Active	Active
	SOC_{min}	Inactive	Inactive	Inactive	Active	Active
	ΔSOC	Active	Active	Active	Inactive	Inactive
	# of iterations	17	32	20	22	30

Table 11: Different starting points optimization results

From Table 11, it is clear that multiple local minima exist when constraints are applied. With all constraints applied three local minima, each with different design solutions, are obtained. The initial point subspaces that lead to different solutions are not as clear as the unconstrained case. Unlike the unconstrained case, the objective function varies significantly with varying initial points. Thus, it is necessary for a designer to try different initial points in order to gain confidence that their solution is the global optimum. Comparing surrogate vs. simulation objective function values for different solutions, it is evident that there is an error between the original and approximated model, as expected. However, the general trends of the objective function are valid. It should be noted that some constraint functions are markedly inaccurate, such that the solution obtained from the surrogate model may violate constraints in the simulation. Further analysis on the feasibility of the surrogate model is discussed in section 6.6. On the other hand, it is interesting to see that the constraint activity varies with different initial points. In fact, three solutions have different combinations of active constraints. The first three

trials give the same solution and FC length, battery weight, and ΔSOC are active. For \mathbf{x}_{0_4} only battery weight and SOC_{min} are active. Note that P_{pa} is constrained by the simple bound for this solution. For the last solution, considered the best design solution obtained, FC length, battery weight, and SOC_{min} are active. It is found that there exists a relationship between SOC_{min} and ΔSOC . When the SOC_{min} constraint is relaxed, ΔSOC becomes active. Further analysis on this behavior will be discussed in the parametric study given in Section 7.1. In general we can conclude that the problem is numerically robust and has good global convergence properties due to the smoothness of the surrogate model.

6.6 Surrogate Model Feasibility

The solution presented in Table 5 indicates the optimal design as obtained through SQP on the surrogate model. This design is considered to be both optimal and feasible for the surrogate model. However, verification is required to determine the feasibility and optimality of the design for the physical model, computed through simulation. To aid this discussion, Table 12 specifies the constraint and objective function values for both the surrogate model and simulation. A percentage difference is also included to elucidate discrepancies between the two models. Several significant observations are obtained through this examination.

The simulation model is infeasible for the optimal design variables derived from the surrogate model. Although this result is discouraging, it highlights the limitation of using surrogate models. In this case, the surrogate model does an inadequate job of approximating the certain constraint function values, resulting in an infeasible solution.

The surrogate model is particularly poor at predicting average parasitic loss, fuel cell system efficiency, oxygen excess ration, and minimum SOC displacement. A possible culprit may be the stochastic nature of the power demand cycle, which creates random sets of constraint function values that are rather discontinuous in nature. The neural network captures general trends for each constraint, but has difficulty outputting accurate values for a specific set of design variables.

In general, the power of surrogate modeling is limited by the accuracy of its approximation. In the case of using neural networks, mean squared error reduces if more neurons and hidden layers

are applied. Yet, this requires significant computational cost, which may not be desirable. Therefore, accuracy vs. cost must be weighed to ascertain the best course of action.

In the case an infeasible solution is found, one may assert more aggressive constraints to enclose the feasible region of the surrogate model to within the feasible region of the physical model. This idea is conceptually illustrated by Figure 14, where the margin of error is defined by how much more aggressive the constraints are made beyond nominal values.

<i>Constraints & Objective</i>	<i>Surrogate Model</i>	<i>Simulation</i>	<i>Abs. Percent Difference</i>
Compressor Surge Condition	-208114.4478	-213263.1605	2.47 %
Max SM Pressure Ratio	1.0541	1.0541	0 %
Min SM Pressure Ratio	1.0257	1.0259	0.02 %
Fuel Cell Stack Length	1.2 m	1.1968 m	0.27 %
Battery Weight	75 lbs	69.8688 lbs	6.84 %
Heat Generated by Stack	5384.2099 W	5183.5372 W	3.73 %
Average Parasitic Loss	5.3579 %	0.52089 %	90.28 %
Fuel Cell System Efficiency	61.9307 %	47.8106 %	22.80 %
Oxygen Excess Ratio	2.1379	3.3361	56.05 %
Max SOC	0.7	0.7	0 %
Min SOC	0.6	0.57131	4.78 %
SOC Displacement	0.0020426	0.097435	4670 %
H ₂ Fuel Consumption	0.0756 kg	0.0756 kg	0 %

Table 12: Comparison of constraint values using surrogate model and simulation. Average compressor to stack power and average efficiency is omitted due to remaining modeling issues.

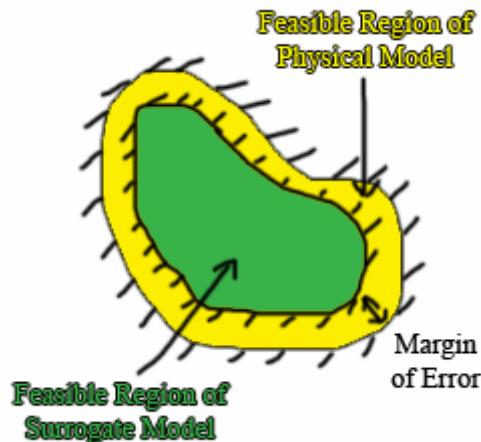


Figure 14: Conceptual depiction of ensuring feasibility for a physical model when using a surrogate model for optimization.

7. Parametric Study

In practice, it is often desirable to optimize more than one design objective, such as total weight, size, efficiency, and fuel economy. The formulation of such a problem is known as a multi-objective optimization problem, which may be solved by parameterizing the constraints and observing relative cost tradeoffs for each objective. The design metrics that are of particular interest to a hybrid fuel cell V2G system are the minimum SOC, battery weight, and fuel cell stack length. In the following sections each of the aforementioned constraints are formulated into objectives and Pareto curves are generated to facilitate analysis.

7.1 Minimum SOC

To increase battery life, it is desirable to regulate SOC to a bounded region, usually characterized by excellent efficiency. For the case given in this study, we wish to regulate SOC to 0.7 while bounding its response between 0.6 and 0.75. Suppose, the lower bound is parameterized such the tradeoffs between fuel consumption and SOC regulation can be determined, depicted by the Pareto front in Figure 15. Increasing the minimum SOC value requires an increase in control action from the fuel cell while decreasing minimum SOC does the converse. This inverse relationship is easily understood, but what becomes particularly interesting is the flat region of the Pareto front. A slope of nearly zero indicates there is a point of diminishing returns for relaxing minimum SOC in order to obtain lower fuel consumption. Observation of activity for these points reveals that minimum SOC becomes inactive and maximum SOC displacement becomes active. Hence, SOC_{\min} dominates ΔSOC_{\max} for $SOC_{\min} > 0.57$, but ΔSOC_{\max} dominates SOC_{\min} for $SOC_{\min} < 0.57$. Although this method has practical use for quantifying an optimal solution, it also provides fascinating insight to the handoff of constraints and their relative importance in different regions of the design space.

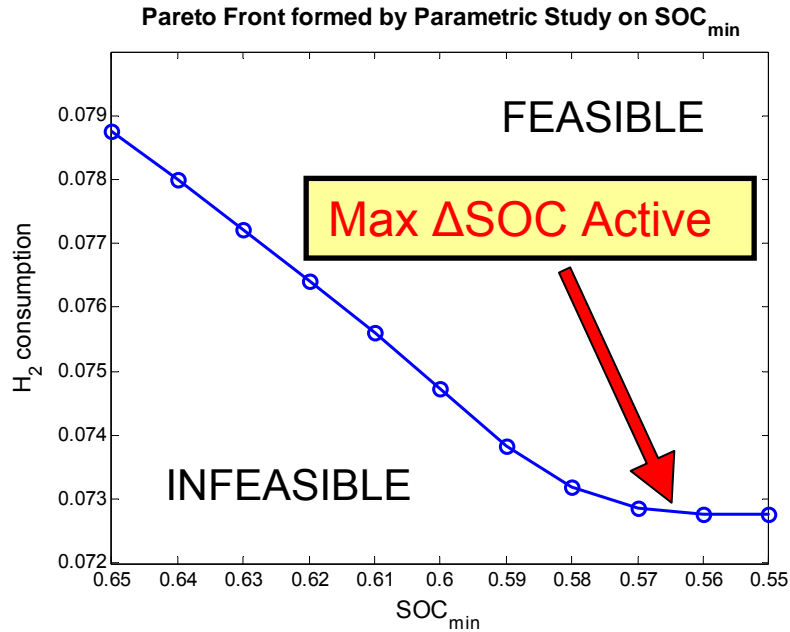


Figure 15: Parametric study on minimum SOC.

7.2 Maximum Battery Weight

For stationary applications, battery weight is not an issue of concern. However, the system proposed in this report describes a power generation device that may be used for both power grid generation and vehicle propulsion. As such, the battery weight should be minimized for fuel economy and vehicle dynamic considerations. A multi-objective problem may be formulated which minimizes both fuel consumption and battery weight. To analyze this optimization problem, battery weight is set as a constraint and parameterized to create a Pareto front shown in Figure 16. Qualitatively, the curve shows a clear tradeoff between minimizing fuel consumption and battery weight. Minimizing battery weight produces a system design which consumes more fuel, but a system that minimizes fuel consumption requires a larger battery. Interestingly, a system with battery weight greater than 87.5lbs does not experience appreciable decrease in fuel consumption. By noting constraint activities, it is observed that ΔSOC_{max} becomes active for solutions with weights greater than 87.5 lbs. Hence, the maximum SOC displacement constraint places a limit on the minimum fuel consumption with respect to increase in battery weight. Knowledge of this behavior may guard against over-designing a system. For example, if a designer conceptually understands that increasing battery weight decreases fuel consumption, they may blindly chose an extremely large battery size. The analysis presented here aims to reveal the subtleties not easily understood intuitively.

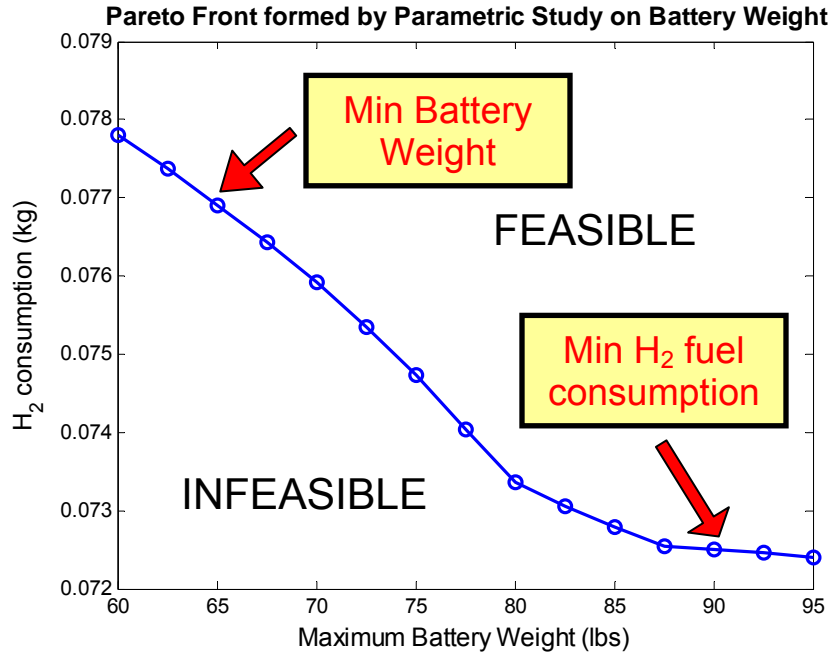


Figure 16: Parametric study on maximum battery weight.

7.3 Maximum Fuel Cell Stack Length

The maximum length available for packaging a fuel cell within a vehicle is limited by the federal standard for highway lane width, as discussed in Section 4.3. Alternative packaging methods may be used to allow for longer stack sizes, such as longitudinal mounting. The design of experiment study and fuel cell efficiency curve indicate a larger fuel cell can produce power more efficiently, at the cost of component size. Suppose it is desired to obtain the most fuel efficient hybrid fuel cell system possible while minimizing stack length. The two objectives form a Pareto front given in Figure 17. Ideally, the optimal solution approaches zero fuel consumption and zero stack length, represented by the origin. However, this point lies in the infeasible space. The boundary between the feasible and infeasible spaces, shown in Figure 17, is often referred to as the Pareto front. Depending on the engineer’s preference for minimum fuel consumption or stack length, an infinite number of optimal solutions are available. However, placing a preference on one objective sacrifices the other. For example, the lowest fuel consumption can be achieved by sacrificing small fuel cell stack length. Conversely, a shorter fuel cell stack consumes a greater amount of fuel. The best solution is usually determined on a case-by-case basis, in which constraints do exist on certain objective.

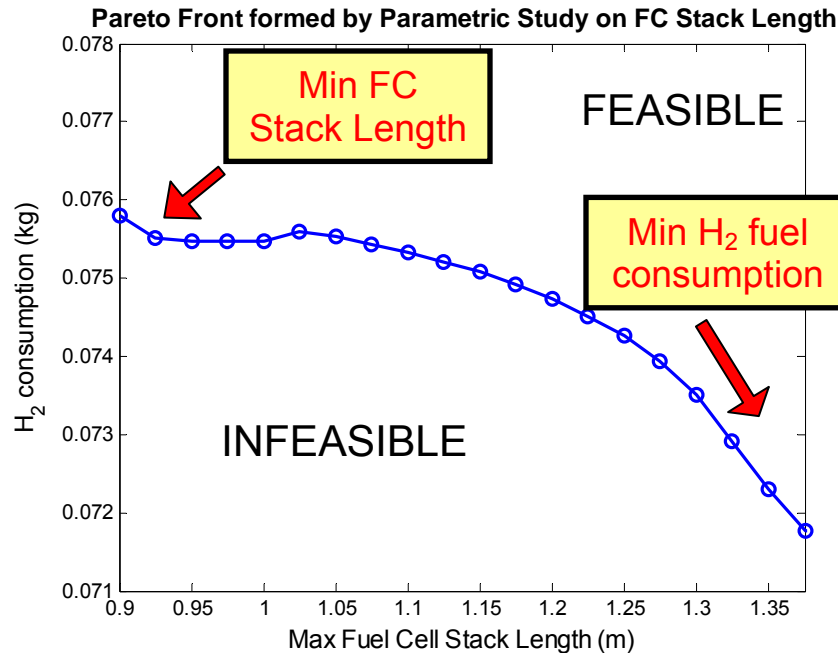


Figure 17: Parametric study on maximum fuel cell stack length.

8. Discussion of Results

From an engineering implementation perspective the design solution suggests the maximum number of fuel cells & battery modules, and the smallest feasible compressor, thus providing maximum efficiency. From a rule-based controller standpoint, the optimal design reduces the fuel cell only power region such that fuel cell usage time is minimized and it is constrained to operate in a region of maximum efficiency. However, this causes the fuel cell system to turn on and off frequently, which may not be desirable due to stack durability issues. The frequency of fuel cell switching modes can be added as a constraints or cost function, which will impose a new type of trade-off. Also, cost, one of the most significant factors in practical engineering design is neglected in this study. The inclusion of a cost function term in the objective would impose a clear trade-off for larger component size designs.

8.1 Design Rules

Based on the above analysis, the following design rules are suggested. (1) A design which minimizes fuel consumption is characterized by maximum fuel cell and battery size within the allowable size and weight constraints. (2) A relatively small compressor maximizes fuel cell system peak efficiency by reducing parasitic losses. (3) A designer should synthesize a controller

which minimizes fuel cell usage and maximizes operating efficiency by assigning P_{pa} and P_{batt} threshold values around the region of maximum efficiency. (4) As discussed in Section 5.2, the sensitivities of the control design variables are larger than the component sizing variables. Thus a designer should carefully tune the control design variables to minimize fuel consumption.

8.2 Model Limitations

The physical model developed by Pukrushpan is based on the assumption of steady-state behavior [7]. However, applying a control scheme that requires on & off switch of the fuel cell would necessitate the creation of a model to sufficiently describe transient behaviors. The development of a high fidelity transient model is necessary for more accurate results; however such a task is beyond the scope of this course project. Despite this inherent limitation, the depth of optimization analysis is not compromised. Surrogate models are intrinsically limited by their fidelity. Notably, the feasibility of a solution obtained using a surrogate model needs to be analyzed carefully, since there approximation error exists between the original and surrogate models.

8.3 Future Work

A logical extension of this work would optimize the same hybrid fuel cell system for an onboard vehicle application, applied to a set of driving cycles. The resulting design can be compared and contrasted to the design suggested in this work to understand the inherent trade-offs between two remarkably different applications. Moreover, a combined system optimization problem can be formulated to determine the optimal design for a hybrid fuel cell system intended for both applications by applying the concept of V2G.

A heuristic control algorithm is selected to provide a framework appropriate for design optimization. Future work may include applying more rigorous control theory, especially with regard to supervisory control. Some ideas that have been presented in the literature include the application of stochastic dynamic programming [3], which would be well suited for grid power demand.

9. Acknowledgements

We would like to extend our gratitude towards Professor Papalambros for his guidance and support. Professor Huei Peng was instrumental in providing the fuel cell system model and we acknowledge his support. We also wish to thank Jeongwoo Han for the many discussions regarding his research and our project work. Dr. Michael Kokkoalaras assisted us with using neural networks for surrogate modeling, which was extremely helpful. Dr. Hosam Fathy provided guidance in formulating our problem and James Allison provided advice on applying analytical target cascading techniques, which we declined to use.

10. References

- [1] L. D. Burns, J. B. McCormick and C. E. Borroni-Bird, "Vehicle of change," *Sci. Am.*, vol. 287, pp. 64-73, 2002.
- [2] J. Han., Optimal design of hybrid and non-hybrid fuel cell vehicles M.S. thesis, University of Michigan, Ann Arbor, 2000.
- [3] Min-Joong Kim and Hwei Peng, "Combined control/plant optimization of fuel cell hybrid vehicles," in *2006 American Control Conference, 14-16 June 2006*, 2006, pp. 6.
- [4] V. Tsourapas and A. Karnik, "Design and Control Optimization of a PEM Fuel Cell," *ME 555 Project Archive*, 2005 [<http://www.optimaldesign.org/archive.html>].
- [5] H. K. Fathy, J. A. Reyer, P. Y. Papalambros and A. G. Ulsov, "On the coupling between the plant and controller optimization problems," in *Proceedings of American Control Conference*, pp. 1864-9.
- [6] L. Guzzella. Control oriented modelling of fuel-cell based vehicles. Presentation in NSF Workshop on the Integration of Modeling and Control for Automotive systems, 1999.
- [7] J. T. Pukrushpan, A. G. Stefanopoulou and H. Peng, *Control of Fuel Cell Power Systems: Principles, Modeling, Analysis and Feedback Design.* , vol. XVII, Springer, 2004, pp. 161.
- [8] Moraal, P. and Kolmanovsky, I. (1999). Turbocharger modeling for automotive control applications. *SAE Paper 1999-01-0908*.
- [9] California ISO: System Status. <http://www.caiso.com/outlook/outlook.html>.
- [10] P. Papalambros and D. Wilde. Principles of Optimal Design. Cambridge University Press., 2nd edition, 2000.